Original Article

Rational Immunoinformatics-Driven Design of Multi-Epitope Vaccine Candidate Targeting EBNA1 and BZLF1 in Epstein–Barr Virus-Associated Gastric Carcinoma

Rachma Greta Perdana Putri[1](0000-0002-6475-8473), Ysrafil Ysrafil[2*](0000-0002-5980-7525), Leony Dwi Rizkita[3] (0000-0003-2576-8529), Annisa Annisa[4](0009-0005-0209-9264), Barkah Djaka Purwanta[5](0000-0003-1133-1158)

[1]Department of pathological Anatomy, Faculty of Medicine, Universitas Ahmad Dahlan, Yogyakarta, Indonesia

[2]Department of Pharmacotherapy, Faculty of Medicine, Universitas Palangka Raya, Palangka Raya, Indonesia

[3]Department of Pharmacology, Faculty of Medicine, Universitas Ahmad Dahlan, Yogyakarta, Indonesia

[4]Department of Histology, Faculty of Medicine, Universitas Ahmad Dahlan, Yogyakarta, Indonesia

[5]Department of Internal Medicine, Faculty of Medicine, Universitas Ahmad Dahlan, Yogyakarta, Indonesia

Correspondence to: Ysrafil, B.Pharm., M.Biomed

Department of Pharmacotherapy, Faculty of Medicine, Universitas Palangka Raya, Palangka Raya, Indonesia

Hendrik Timang Street, Palangka Raya, Kalimantan Tengah, Indonesia

https://orcid.org/0000-0002-5980-7525

E-mail: ysrafil@med.upr.ac.id

Running Title: **Multi-epitope vaccine peptide for EBV-related gastric cancer**

ABSTRACT

Background and Aim: EBVaGC represents a distinct molecular subtype of gastric cancer, accounting for approximately 10% of all cases. Among EBV-encoded antigens, EBNA1 and BZLF1 have emerged as promising targets for vaccine development due to their critical roles in viral persistence and lytic reactivation, respectively. In this study, we rationally designed multi-epitope vaccine peptide candidate targeting these key proteins in EBVaGC.

Results: A large number of CTL, HTL, and LBL epitopes were identified from both proteins. Subsequently, the top three epitopes in each category epitopes for each precursor protein were selected according to percentile rank, antigenicity, immunogenicity, non-allergenicity, and non-toxicity to further use in constructs. The selected HTL epitopes also found could induce cytokines responses such as IFN-γ, IL-2, IL-4, and IL-10. A population coverage analysis reveal that the selected epitopes showed a high global population coverage of 97.25%, indicating broad

applicability across diverse populations. Furthermore, in this study three MEVP constructs were designed and exhibiting favorable antigenic, non-allergenic, and non-toxic properties. Among them, MEVPC demonstrated superior physicochemical characteristics, including a lower instability index and a higher aliphatic index, supported by better structural validation (ProSA Z-score, ERRAT, and Ramachandran plot). Molecular docking analysis revealed that all constructs bind effectively to TLR-9, with MEVPC showing the strongest docking score (−131.5±2.0 kcal/mol). However, MM/GBSA analyses indicated that MEVPA–TLR9 had the highest binding affinity (−62.15 kcal/mol). Contrarily, molecular dynamics simulations confirmed that MEVPA–TLR9 was the most stable complex (RMSD ~1.0–1.4 nm), whereas MEVPC exhibited high instability despite having the highest number of hydrogen bonds. Immune simulation of the MEVPC hypothesis generated strong and sustained immune responses, including elevated IgG1/IgG2, IFN-γ, IL-4, and memory T- and B-cell formation. Conclusion: MEVPA shows the highest structural stability, while MEVPC demonstrates powerful characteristics and strong immunogenic potential, supporting their promise as EBVaGC vaccine candidates.

Keywords: Epstein-Barr virus; vaccine; Gastric cancer, immunoinformatics; EBNA1 and BZLF1

1. Introduction

Epstein-Barr virus–associated gastric carcinoma (EBVaGC) is a distinct molecular subtype of gastric cancer that accounts for approximately 5–10% of all gastric carcinoma cases. This subtype has a characteristic molecular, histological, and immunological profile and is often associated with epigenetic alterations, immune pathway activation, and specific mutations. EBVaGC has characteristic molecular features, such as the CpG island methylator phenotype (CIMP) and mutations in the PIK3CA and ARID1A genes, as well as the expression of latent viral products such as EBNA1 and LMP2A, which trigger epigenetic changes and inhibit apoptosis through the NF-κB pathway. [1–3]

The treatment of EBVaGC primarily involves surgical resection, chemotherapy, and, in some cases, immunotherapy. Recent studies have explored the efficacy of immune checkpoint inhibitors, such as pembrolizumab, in EBVaGC, showing promising results due to the immunogenic nature of these tumors.[4] Preventive strategies for EBV-associated disease are limited, primarily because of the lack of an effective EBV vaccine. Although research has developed an EBV vaccine, challenges persist, including the need for a vaccine that induces a robust T cell-mediated immune response.[5] In addition to preventive purposes, vaccine development has also been carried out for therapeutic effects, including the treatment of EBV-associated malignancies, with promising potential by targeting the viral glycoprotein gp350 as well as latent and lytic proteins.[6]

However, these efforts do not appear to have had a significant impact on the development of preventive and therapeutic vaccines, including those targeting EBVaGC. No therapeutic vaccine for Epstein–Barr virus (EBV) is currently approved, although several candidates targeting EBV-associated malignancies, particularly nasopharyngeal carcinoma, have shown safety in clinical trials. mRNA-based vaccines are especially promising due to their ease of production and tolerability, with ongoing trials exploring efficacy in refractory EBV-related cancers. Advances in viral vectors, T-cell-stimulating adjuvants, structural biology-guided antigen design, and mucosal delivery offer new avenues for effective EBV vaccine development.[7] Furthermore, to enhance vaccine efficacy, recent approaches have focused on the development of multiepitope vaccines that use immunodominant viral antigens.

The development of vaccines targeting immunodominant epitopes derived from Epstein–Barr virus (EBV) proteins represents a promising strategy to address the need for more effective therapeutic and preventive

interventions. Among the potential targets, Epstein–Barr nuclear antigen 1 (EBNA1) and BZLF1 have emerged as particularly attractive candidates for vaccine design against EBV-associated malignancies. EBNA1 is consistently expressed across all EBV-associated cancers and plays a pivotal role in viral genome maintenance and immune evasion, making it an ideal target for inducing robust and sustained T-cell responses.[8] In contrast, BZLF1, an immediate-early lytic protein, is capable of eliciting strong $CD4^+$ and $CD8^+$ T-cell responses prior to the establishment of viral latency, thereby providing a critical window for early immune intervention. Preclinical studies have demonstrated that dendritic cell-based vaccines expressing BZLF1 can induce antigen-specific T-cell responses and delay the onset of EBV-related lymphoproliferative disorders in murine models.[9] Several vaccine candidates have been developed to prevent EBV infection. A vaccine candidate targeting EBV-associated lymphoma incorporated multiple EBV antigens derived from both the lytic and latent phases, including BZLF1, EBNA1, EBNA3B, and gH/gL, to achieve optimal protective efficacy. These multivalent vaccines have been assessed in humanized mouse models of EBV-induced fatal B-cell lymphoma. Furthermore, a separate study examined a heterologous prime–boost vaccination strategy targeting EBV nuclear antigen 1 (EBNA1), where EBNA1 was either directed to the DEC205 receptor on dendritic cells or expressed via a recombinant modified vaccinia virus Ankara (MVA) vector. This vaccination approach enhanced T-cell responses in mice and conferred protection against EBNA1-expressing T- and B-cell lymphomas. EBNA1 has also emerged as a promising vaccine candidate for nasopharyngeal carcinoma (NPC) and has progressed to phase I clinical evaluation. A phase I trial evaluated a recombinant modified vaccinia virus Ankara (MVA-EL) vaccine encoding an EBNA1/LMP2 fusion protein designed to enhance T-cell immunity against these EBV antigens. The results demonstrated that the majority of patients developed increased antigen-specific T-cell responses following vaccination.[10–12] Collectively, these findings highlight the potential advantage of simultaneously targeting both latent and lytic EBV proteins to enhance vaccine efficacy against EBV-associated gastric carcinoma. Notably, the epitope selection strategy employed in this study differs from those commonly used in nasopharyngeal carcinoma (NPC). In NPC, which is typically characterized by latency type II infection, tumor cells predominantly express latent membrane proteins (LMPs) as well as envelope glycoproteins such as gp350 and gp42; consequently, these antigens are frequently prioritized in NPC-focused vaccine development.

Advancements in technology have enabled the rational design of vaccine peptides through computational methods and immunoinformatics approaches, thereby minimizing trial-and-error processes and substantially reducing the cost and time associated with drug development by enabling in silico simulations prior to experimental validation. The approach allows viral proteome scanning to identify highly antigenic, cross-population/promiscuous HLA B-cell and T-cell epitopes, minimize non-specific epitopes, and design combined sequences (multi-epitope fusion proteins) with linkers and immunogenicity-enhancing elements. This method has proven efficient for generating multiepitope antigen candidates that can subsequently be produced recombinantly and stimulate antibody and immune responses against cancer.[13,14]

Several studies have demonstrated the efficacy of multiepitope vaccine design in cancer and infectious disease models. Safavi et al. (2019) reported that a multiepitope peptide vaccine targeting acrosin binding protein (ACRBP) and synaptonemal complex protein 1 (SYCP1) elicited robust humoral and cellular immune responses in C57BL/6 mice, including elevated IgG1/IgG2a levels and increased IL-4 and IFN-γ production. In a B16-F10 melanoma model, vaccination resulted in a 43–50% reduction in tumor volume and prolonged survival by 5–6 days,

demonstrating its prophylactic potential.[14] Similarly, Qiu et al. (2015) showed that a multiepitope vaccine against norovirus using the same approach stimulated high levels of IgG and IgA, highlighting the versatility and immunogenicity of this vaccine design strategy.[15]

Based on the urgency of EBVaGC prevention and treatment, as well as evidence that an immunoinformatics-based multiepitope approach can create accurate vaccine, this study developed a multiepitope vaccine targeting the immunodominant epitopes of EBNA-1 and BZLF1 to detect EBV-related gastric carcinoma.

2. Material and Methods

2.1 Protein selection and sequence retrieval

A comprehensive literature review was conducted to identify experimentally validated proteins of Epstein-Barr virus (EBV). Based on this assessment, two proteins were selected for further analysis: Epstein-Barr nuclear antigen-1 (EBNA-1) and BamHI Z fragment leftward open reading frame 1 (BZLF1). The amino acid sequences of these proteins were retrieved from the National Center for Biotechnology Information (NCBI) database in FASTA format. For the preliminary evaluation, antigenicity was predicted using the VaxiJen v2.0 web server with a threshold value set at 0.40.[16]

2.2 In Silico Prediction of Immunodominant CTL Epitopes

Cytotoxic T lymphocyte (CTL) binding epitopes of the two selected proteins were predicted using the Immune Epitope Database (IEDB). The allele setting was set to the entire HLA allele reference set. Epitopes with a percentile rank of less than 2% were prioritized for further analysis. Each predicted epitope was subsequently evaluated for allergenicity, antigenicity, and toxicity. Allergenicity was assessed using two validated online predictors, AllergenFP v1.0 and AllerTOP v2.0, both of which provide reliable accuracy. Antigenicity was determined using VaxiJen v2.0, applying the virus model with a threshold value of 0.40. Toxicity analysis was performed with ToxinPred, employing the default support vector machine (SVM) settings based on the Swiss-Prot database. [13,17,18]

2.3 In Silico Prediction of Immunodominant HTL Epitopes and Cytokine Induction Analysis

Helper T lymphocyte (HTL) epitopes were predicted using the Immune Epitope Database (IEDB) tool, and epitopes with percentile ranks <2% were selected for further analysis. The allele setting was set to all of HLA allele reference set. The shortlisted epitopes were subsequently evaluated for allergenicity, antigenicity, and toxicity. To assess their immunomodulatory potential, all selected MHC II epitopes were analyzed for their ability to induce cytokine responses, including IFN-γ, IL-4, and IL-10. Cytokine induction was predicted using SVM-based online tools including IFN-epitope, IL4pred, and IL10pred web tools, with default threshold parameters applied for each prediction model. [13,19]

2.4 In Silico Prediction of Immunodominant Linear B- lymphocyte Epitopes

Linear B- lymphocyte (LBL) epitopes were predicted using the ABCpred server with an epitope length of 16 amino acids and a screening threshold of 0.51, with the Overlapping filter set to ON mode. The epitope with the highest prediction score was designated as the immunodominant B-cell epitope for multiepitope vaccine peptide (MEVP) construction. All predicted epitopes were subsequently evaluated for allergenicity, antigenicity, and toxicity using established online prediction tools. [20]

2.5 Population Coverage Analysis

The purpose of this analysis was to determine the extent of global population coverage of the selected epitopes, with

particular emphasis on helper T lymphocyte and cytotoxic T lymphocyte epitopes intended for incorporation into the vaccine construct across diverse geographical regions. Population coverage was calculated using the Immune Epitope Database Population Coverage tool (https://tools.iedb.org/population/), applying a combined analysis of major histocompatibility complex class I and class II alleles, based exclusively on the identified alleles associated with the selected epitopes. To ensure that the estimation was comprehensive and representative, all available regional and ethnic population datasets were included in the analysis. The resulting data were subsequently visualized using MapChart to illustrate the predicted population coverage across different countries as well as at the global level.[21]

2.6 Construction of Multi-epitope Vaccine Peptide

The selected immunodominant epitopes from CTLs, HTLs, and LBLs were utilized in the construction of a multi-epitope Vaccine peptide (MEVP) for therapeutical and preventive vaccine candidate. To enhance immunogenicity and effectiveness, additional sequences were incorporated, including adjuvant and PADRE sequences. Specific linkers were employed to connect the epitopes: AAY linkers for CTL epitopes, GPGPG linkers for HTL epitopes, KK linkers for LBL epitopes, and an EAAAK linker to fuse the adjuvant with the PADRE sequence. A 6×His tag was added at the C-terminal to facilitate downstream applications.

In this study, we also assessed the influence of adjuvant selection and epitope positioning within the construct on vaccine efficacy. Accordingly, three multi-epitope vaccine peptide (MEVP) designs were generated by varying both the adjuvant type and the sequence arrangement. Two adjuvants were employed: the 50S ribosomal protein and human β-defensin (hBD). The constructs were assembled in distinct schematic configurations to systematically evaluate how sequence positioning impacts the elicited immune response.[22–24] The overall schematic design of the MEVP constructs is presented in **Figure 1**.

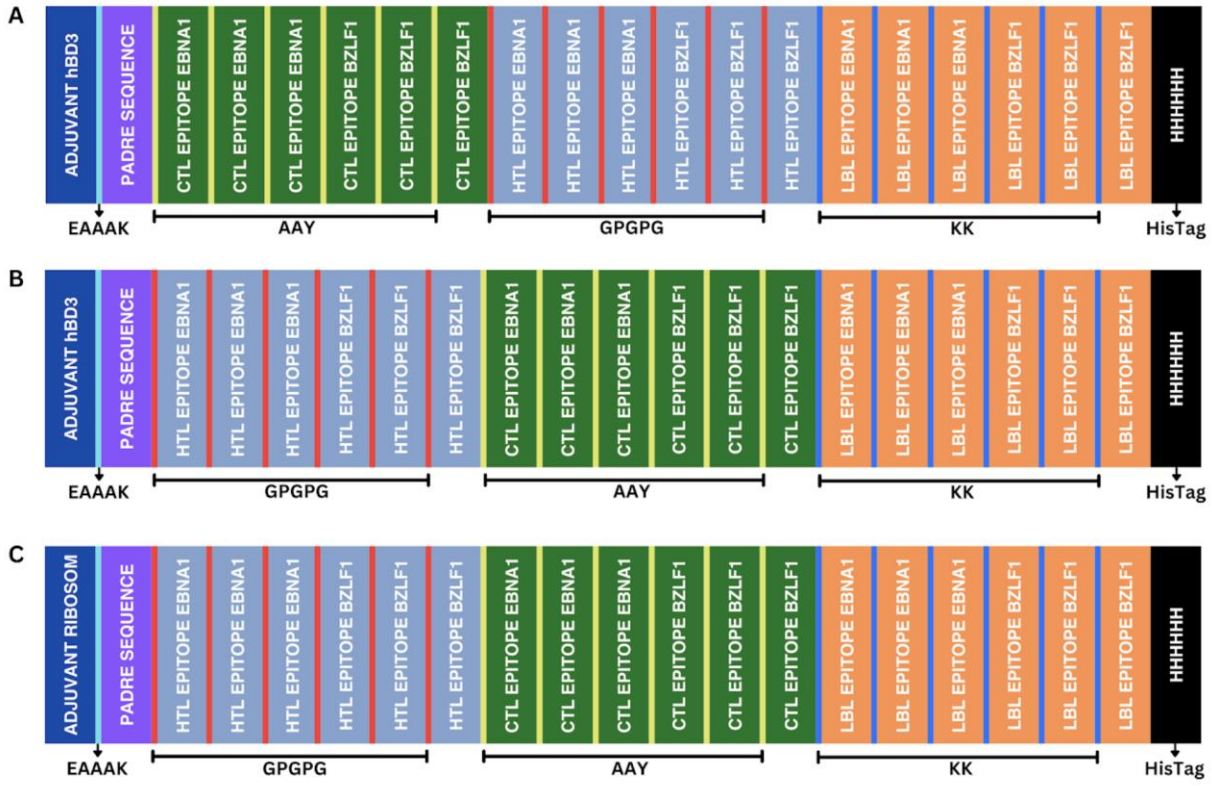


Figure 1. Rationally designed architectures of the three multi-epitope vaccine candidates for EBVaGC (MEVPA, MEVPB, and MEVPC), illustrating their study-specific organization of antigen-derived epitopes, linkers, and adjuvant modules. The distinct molecular configurations highlight the tailored epitope arrangements and adjuvant compositions underlying the comparative vaccine designs developed in this study.

2.7 Physicochemical and Immunoinformatic Characterization of the MEVP

a. Physicochemical Analysis

The physicochemical properties of the multi-epitope vaccine peptide (MEVP) constructs were analyzed using the *ExPASy-ProtParam* server. The amino acid sequences were directly pasted into the input field and analyzed using default settings. Parameters including molecular weight, theoretical isoelectric point (pI), instability index, aliphatic index, and grand average of hydropathicity (GRAVY) were calculated to evaluate the basic structural and stability characteristics of each construct. [25]

b. Immunological Profiling

The immunological characteristics of the MEVP constructs were evaluated based on antigenicity, allergenicity, and toxicity. The amino acid sequences were directly pasted into the input field and analyzed using default settings. Antigenicity was predicted using *VaxiJen v2.0* (threshold: 0.4; tumor model) to assess the potential of the constructs to induce an immune response. Allergenicity was assessed using *AllerTOP v2.0* to determine the likelihood of allergenic reactions. Toxicity was evaluated using *ToxinPred* to ensure the safety profile of the designed peptides. [13,17,18]

c. Solubility Prediction

The solubility of the MEVP constructs upon overexpression was predicted using the *Protein-Sol* web server. The amino acid sequences were pasted into the input field and analyzed using default parameters to estimate their solubility and assess potential expression feasibility in heterologous systems. [26]

d. Secondary Structure Analysis

The secondary structure of the MEVP was analyzed using PSIPRED (PSI-BLAST-based secondary structure prediction) and SOPMA. Default parameters were applied for SOPMA, while PSIPRED provided graphical visualization of the predicted secondary structural elements, including α-helices, β-strands, and coils.[27,28]

2.8 Tertiary Structure Modeling, Refinement, and Validation of the MEVP

The tertiary structures of the MEVP constructs (MEVPA, MEVPB, and MEVPC) were initially generated using I-TASSER, a widely recognized and top-ranked server for automated protein structure prediction.[29] The preliminary models obtained were subsequently refined employing the GalaxyRefine server to improve structural accuracy and stereochemical quality.[30] The validity and reliability of the refined 3D model of MEVP were assessed using multiple structural evaluation tools: ERRAT and Ramachandran plot via SAVES v6.0 for stereochemical validation, and ProSA for overall model quality assessment based on Z-score and energy profiles. Finally, the three-dimensional conformation of the protein construct was visualized and analyzed using PyMOL molecular graphics software.[13,20,23,31]

2.9 Analysis of discontinuous B-cell epitope

Discontinuous B-cell epitopes of constructed vaccine were predicted using the ElliPro tool available on the IEDB platform (http://tools.iedb.org/ellipro/), based on the three-dimensional (3D) structure of the protein. The analysis was

performed using default parameters, with a minimum score threshold of 0.5 and a maximum distance of 6 Å between neighboring residues.

2.10 Protein disulfide engineering

Disulfide engineering involves identifying and modifying potential residues in highly flexible regions of a protein sequence to create new disulfide bonds. These bonds improve the geometric conformation of the protein and enhance its stability. To achieve this, the Disulfide by Design 2.0 (DbD2) online server was utilized, accessible at http://cptweb.cpt.wayne.edu/DbD2/index.php. This tool identifies pairs of residues that can form disulfide bonds when each residue is mutated to cysteine. The use $\chi 3$ value was −87° to +97° (set to 30), Cα Cβ–Sγ angles (114.6°) were set to 10, and the energy value was <4.0 kcal/mol.[32]

2.11 Docking Simulation and Interaction Analysis of MEVP–TLR9 Complexes

Molecular docking was conducted to evaluate the interaction between the multiepitope Vaccine peptide (MEVP) and the host receptor toll-like receptor 9 (TLR9). The crystal structure of TLR9 was retrieved from the Protein Data Bank (PDB ID: 3WPF) (https://www.rcsb.org) and further refined using MODELLER 10.8 integrated within UCSF Chimera 1.19. Prior to docking, the protein structure was prepared using BIOVIA Discovery Studio by removing non-protein molecules from the co-crystal structure. Polar hydrogen atoms were added to the 3D models of both TLR9 and the MEVPs. Subsequently, the active binding sites of TLR9 and the MEVP constructs were determined using PrankWeb (https://prankweb.cz/), a binding site prediction tool based on P2Rank, a machine learning–driven method for identifying ligand-binding sites from protein structures.[33]Docking simulations were performed using HADDOCK 2.4 (https://wenmr.science.uu.nl/haddock2.4/), which integrates biochemical and biophysical information for flexible docking. The best-ranked docked models were subsequently refined to improve complex stability, and the reported docking scores were based on the refined complexes. Furthermore, the resulting MEVP–TLR9 complexes were analyzed using PRODIGY (https://wenmr.science.uu.nl/prodigy/) to estimate binding affinity (ΔG), dissociation constant (Kd) at a given temperature, and interfacial contacts. Finally, the refined complexes were visualized, and interaction mapping was performed using the PDBsum server (https://www.ebi.ac.uk/thornton-srv/databases/pdbsum/) and PyMOL molecular graphics software.[16]

2.12 Molecular dynamics Simulation and MM-GBSA Free Energy Analysis

Molecular dynamics simulations were performed using a DELL Optiplex 7000 Tower workstation (Intel Core i9-12900K, 64 GB RAM, 2 TB + 1 TB SSD storage) equipped with an Nvidia GeForce RTX 3070 8 GB GPU. The TLR9 protein structure was first refined using MODELLER 10.8 integrated within UCSF Chimera 1.19.[34,35] System preparation was carried out using GROMACS version 2026.0, where protein topology was generated using the *pdb2gmx* module with the OPLS-AA/L force field.[36] The system was subsequently solvated, followed by the addition of Na^+ and Cl^- ions to achieve a physiological concentration of 0.15 M. The simulation workflow included energy minimization, equilibration, and production phases, with all preparation steps automated using CHAPERONG.[37] The production run was conducted for 100 ns at a constant temperature of 310.15 K (37 °C). Trajectory analyses included *root mean square deviation* (RMSD) of the backbone, *root mean square fluctuation* (RMSF) of Cα atoms, *solvent-accessible surface area* (SASA), and *radius of gyration* (Rg), which were visualized as plots using Gnuplot.

2.13 Codon Optimization and In silico cloning

Codon optimization of the MEVP sequence was performed using the Java Codon Adaptation Tool (JCat) to

enhance translational efficiency in a prokaryotic expression system. *Escherichia coli* K-12 was selected as the host strain, and the optimization process incorporated Rho-independent transcription terminators and prokaryotic ribosome binding sites while avoiding undesirable motifs, such as prokaryotic ribosomal binding site conflicts and cleavage sites for restriction enzymes EcoRI and BamHI. The optimized cDNA sequence was designed in reverse orientation to the peptide construct, with EcoRI and BamHI recognition sites introduced at the N- and C-termini, respectively, to facilitate directional cloning. The optimized gene sequence was subsequently inserted in silico into the pET-28a(+) expression vector using SnapGene software, enabling virtual assessment of cloning accuracy and construct integrity prior to laboratory implementation.[13]

2.13 Immune simulation

Immune response simulations were performed using the C-IMMSIM server (https://kraken.iac.rm.cnr.it/C-IMMSIM/), a widely utilized in silico tool for predicting vaccine-induced immunogenicity. In the simulations, the multiepitope vaccine construct was administered in a prime-boost regimen consisting of three injections at four-week intervals on days 0, 28, and 56. This protocol allowed for the assessment of both primary and secondary immune responses, including the dynamics of B-cell and T-cell populations, antibody titters, and cytokine profiles after injection. It provided a predictive evaluation of the vaccine's immunostimulatory potential prior to in vivo experimentation.[13]

3. Results

Retrieval and Evaluation of EBNA1 and BZLF1

Protein candidates identified as precursors for vaccine design were retrieved from the NCBI database, specifically EBNA1 (YP_401677.1) and BZLF1 (YP_001129467.1). The amino acid sequences were obtained in FASTA format for downstream computational analysis. Antigenicity prediction using VaxiJen 2.0 demonstrated that both proteins exhibited antigenic potential, with scores exceeding the default threshold of 0.40 (Table S1). Allergenicity assessment through AllerTOP and AllergenFP produced consistent results for BZLF1, which was classified as a probable non-allergen by both tools. However, EBNA1 displayed discordant predictions, being categorized as a probable non-allergen by AllerTOP but as a probable allergen by AllergenFP. Physicochemical characterization performed using ProtParam revealed that BZLF1 comprises 245 amino acids and possesses an instability index of 63.09, indicating an unstable nature. Conversely, EBNA1 exhibited an instability index of 37.52, classifying it as stable.

Prediction of Immunodominant CTL Epitopes

$CD8^+$ cytotoxic T lymphocyte (CTL) epitopes were predicted by screening candidate peptides for their binding affinity to major histocompatibility complex class I (MHC-I) molecules, which are responsible for presenting foreign antigens to CTLs.[38] The predicted epitopes were subsequently evaluated for antigenicity, immunogenicity, allergenicity, and toxicity to identify optimal candidates for incorporation into a multi-epitope vaccine peptide (Table S2). Based on these analyses, three epitopes each were selected from BZLF1 and EBNA1, prioritizing those with non-allergenic and non-toxic properties, strong antigenic and immunogenic potential, and favorable percentile ranks (lower values indicating higher predicted binding affinity and desirability). Notably, the epitope ^{154}APARRTRKPL^{163} from BZLF1 and ^{518}YNLRRGTAL^{526} from EBNA1 demonstrated the highest antigenicity scores, making them strong candidates in vaccine constructions.

Prediction of Immunodominant HTL Epitopes and Cytokine Induction

Helper T lymphocyte (HTL) epitopes, each comprising 15 amino acids, were predicted based on their binding affinity to MHC class II molecules, which present foreign antigens to $CD4^+$ T cells and are expressed on the surface of antigen-presenting cells (APCs). Among the predicted candidates, the epitopes ^{71}PQGQLTAYHVSAAPT^{85} from BZLF1 and ^{474}SNPKFENIAEGLRAL^{489} from EBNA1 exhibited the highest antigenicity scores. The shortlisted HTL epitopes were further assessed for their ability to stimulate cytokine responses, specifically IFN-γ, IL-4, and IL-10 (Table S3). Cytokine induction is particularly relevant for vaccine, as measuring specific cytokine responses enables differentiation of EBV-specific immune responses from those elicited by unrelated pathogens and stimulates the activation of specific immune effector cells. For instance, interferon-gamma (IFN-γ) promotes the activation of cytotoxic $CD8^+$ T cells and enhances antigen presentation, which is essential for targeting intracellular pathogens and tumor cells. Similarly, interleukin-4 (IL-4) drives B-cell proliferation and differentiation, facilitating robust antibody production and class switching. The balanced induction of Th1- and Th2-type cytokines ensures a comprehensive immune response, enhancing long-term immunological memory and increasing the prophylactic and therapeutic potential of vaccines.[39] Based on antigenicity, immunogenicity, cytokine-inducing potential, percentile rank, and favorable non-allergenic and non-toxic profiles, the three most promising HTL epitopes from each of BZLF1 and EBNA1 were selected for further construct design.

Prediction of Immunodominant Linear B- lymphocyte Epitopes

Prediction of linear B-cell (LBL) epitopes was conducted given their role as the primary targets of antibody recognition, making their selection crucial for the development of vaccine capable of detecting infection since it could recognize antigen.[40] LBL epitopes from BZLF1 and EBNA1 were predicted using the ABCpred server, which employs an artificial neural network (ANN) algorithm to identify epitopes of fixed length (16 amino acids) with reported accuracy ranging from 65% to 93%. In line with previous epitope analyses, the predicted epitopes were further evaluated for antigenicity, allergenicity, and toxicity profiles. This assessment identified multiple epitopes with desirable characteristics, including antigenic, non-allergenic, and non-toxic properties. Among these, ^{151}PAAAPARRTRKPLQPE^{166} from BZLF1 and ^{510}YGGSKTSLYNLRRGTA^{525} from EBNA1 exhibited the highest antigenicity scores. To prevent excessive construct size in the final multi-epitope vaccine peptide (MEVP), only the top three epitopes from each protein were selected based on their antigenic potential and safety profiles (Table S4).

Population coverage

The population coverage analysis demonstrated a high and broadly distributed global reach of the selected epitopes, with an overall estimated world population coverage of 97.25% (Figure 2). Regionally, the highest coverage was observed in North America (99.26%), West Africa (99.57%), and East Africa (98.16%), indicating strong representation of the selected epitopes across these populations. Similarly, Europe (97.88%) and East Asia (97.26%) also exhibited high coverage, reflecting the wide applicability of the vaccine construct in these regions. Moderately high coverage was identified in Oceania (96.09%), North Africa (95.96%), Southeast Asia (94.53%), and Southwest Asia (94.59%), suggesting substantial but slightly variable epitope representation. In contrast, relatively lower coverage was observed in South Asia (91.8%) and Northeast Asia (92.49%), although these values still indicate a generally acceptable level of population inclusion. Overall, the results highlight that the selected HTL and CTL epitopes provide extensive global population coverage, supporting their potential suitability for inclusion in a broadly

effective multi-epitope vaccine design.

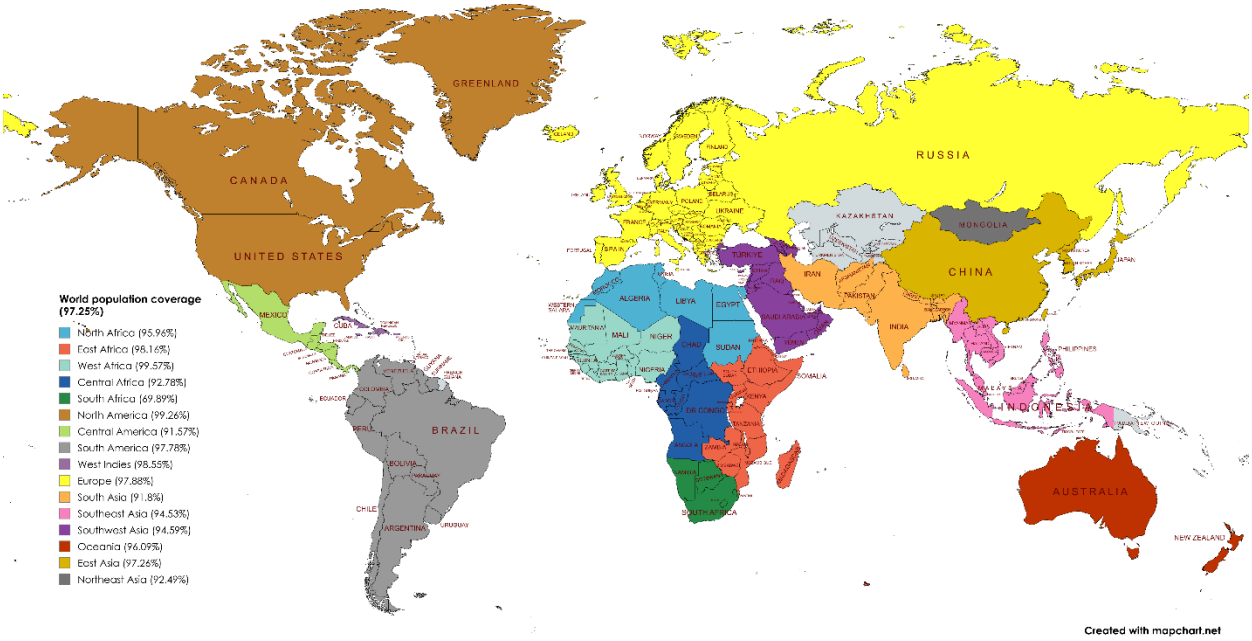


Figure 2. Population coverage of selected CTL and HTL epitopes visualized by MaChart reflect high coverage in population in world wide.

Construction and Evaluation of Multi-Epitope Vaccine Peptide (MEVP)

Three MEVP constructs were designed with variations in adjuvant incorporation and epitope arrangement to obtain the optimal sequence for detecting EBV-associated gastric carcinoma (EBVaGC). Human β-defensin 3 (hBD-3) was fused to the N-terminal region of the construct as a molecular adjuvant to enhance immunogenicity. Due to its human origin, hBD-3 offers a favorable safety profile, making it a suitable built-in adjuvant for vaccine.[41,42] Similar to hBD-3, the L7/L12 ribosomal was incorporated at the N-terminal region in an alternative MEVP construct to enhance its effectiveness. L7/L12 has frequently been employed as a molecular adjuvant in vaccine design due to its ability to potentiate immune responses, thereby improving the overall efficacy of multi-epitope constructs.

The three MEVP constructs are presented in Figure S1, with MEVPA and MEVPB each comprising 371 amino acids, while MEVPC contains 456 amino acids. Antigenicity prediction revealed scores greater than 0.4 for all constructs, confirming their antigenic potential, while allergenicity predictions classified all constructs as non-allergenic. The physicochemical properties, summarized in Table 1, demonstrated that MEVP-C had the highest molecular weight (46,807.28 Da) due to its greater amino acid content; nevertheless, this value remained below the acceptable threshold of 110 kDa.[43] The instability index indicated that MEVPA (40.04) and MEVPB (40.19) were unstable, whereas MEVPC (33.13) was classified as stable. The aliphatic index values were 59.70, 59.70, and 71.54 for MEVPA, MEVPB, and MEVPC, respectively, suggesting higher thermal stability for MEVPC. The GRAVY scores were –0.536 (A), –0.536 (B), and –0.316 (C), indicating that all constructs are hydrophilic, with MEVPA and MEVPB being more hydrophilic than MEVPC. The solubility of the MEVP constructs was evaluated using the Protein-Sol server. All constructs were predicted to be soluble, with scores of 0.692 for MEVPA, 0.692 for MEVPB, and 0.527 for MEVPC, all exceeding the default solubility threshold of 0.45, thereby indicating favorable solubility profiles

(Figure S2).

Table 1. Antigenicity, allergenicity, and physicochemical characteristic of the construct

Construction	Antigenicity	Allergenicity	Molecular weight	Theoretical pI	Ext. coefficient	Est. half life	Instability index	Aliphatic index	GRAVY
A (adjuvant hBD) 371 AA	0.5490	Probable non-allergen	38527.99	9.93	35.340 34.840	Mammals, in vitro: 30 h yeast, in vivo : >20 h; E.coli, in vivo: >10 h	40.04 unstable	59.70	-0.536
B (adjuvant hBD) 371 AA	0.5067	Probable non-allergen	38527.99	9.93	35.340 34.840	Mammals, in vitro: 30 h yeast, in vivo : >20 h; E.coli, in vivo: >10 h	40.19 unstable	59.70	-0.536
C (adjuvant ribosom) 456 AA	0.4638	Probable non-allergen	46807.28	9.18	31.985 31.860	Mammals, in vitro: 30 h yeast, in vivo : >20 h; E.coli, in vivo: >10 h	33.13 stable	71.54	-0.316

pI, isoelectric point; GRAVY, grand average of hydropathicity; AA, amino acid; E. coli, Escherichia coli.

Analysis of Secondary Structure of MEVP construct

The secondary structures of the MEVP constructs were predicted using PSIPRED (Figure S3) and SOPMA (Figure S4). SOPMA analysis showed that MEVPA (371 amino acids) consisted of 35 α-helices (9.43%), 26 extended strands (7.01%), no β-turns, and 310 random coils (83.56%). MEVPB (371 amino acids) contained 101 α-helices (27.22%), 44 extended strands (11.86%), no β-turns, and 226 random coils (60.92%). MEVPC (456 amino acids) was composed of 160 α-helices (35.09%), 47 extended strands (10.31%), no β-turns, and 249 random coils (54.61%). Compared to MEVPA, constructs B and C exhibited a higher proportion of α-helices and extended strands, suggesting more favorable and stable secondary structures. A high proportion of α-helices and β-strands in MEVPC, compared with the other constructs, indicates a superior structural profile, as these elements contribute to extensive hydrogen bonding, which stabilizes the overall protein structure and promotes strong interactions with antibodies.[44]

Tertiary Structure Modeling, Refinement, and Validation of the MEVP

The tertiary structures of MEVPA, MEVPB, and MEVPC were modeled using the I-TASSER server, which generated five models for each construct. The most reliable models were selected based on their C-score, ranging from –5 to +2, with higher values indicating greater confidence in the predicted structure.[45] The top-ranked models were model 3 for MEVPA (C-score: –0.67), model 2 for MEVPB (C-score: –0.92), and model 2 for MEVPC (C-score: –1.33). The

selected 3D models were subsequently refined using the GalaxyRefine server. Model quality was evaluated based on RMSD (lower values reflect minimal structural deviation and improved reliability) and GDT-HA (higher values indicate better structural similarity and accuracy), as summarized in Table S5. The refined tertiary structures of the three MEVP constructs are presented in Figure 3A–C.

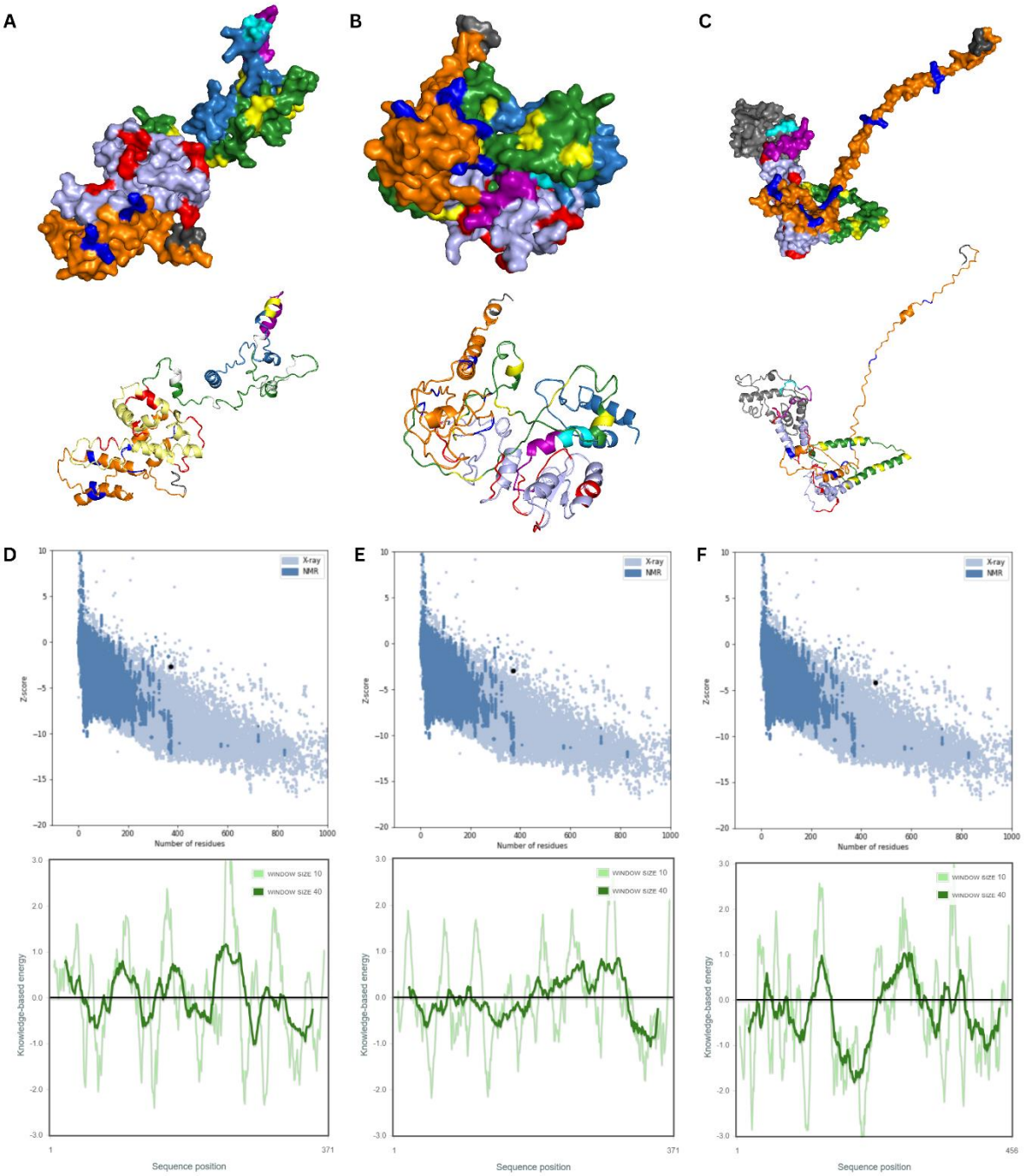


Figure 3. (A–C) Predicted three-dimensional (3D) structures of the MEVP constructs (MEVPA, MEVPB, and MEVPC); (D–F) ProSA-web validation results of the respective constructs, showing the overall model quality based on Z-score analysis.

The refined MEVP constructs were further validated using ProSA-web and the SAVES v6.0 server (ERRAT and Ramachandran plot analyses). As shown in Figure 3D-F, the ProSA Z-scores of MEVPA, MEVPB, and MEVPC were –2.71, –2.91, and –3.33, respectively, values consistent with native proteins of comparable size. Furthermore, ERRAT analysis indicated quality factors of 71.98, 73.52, and 75.00 for MEVPA, MEVPB, and MEVPC, respectively, all exceeding the reliability threshold of 50, thereby confirming acceptable structural models.[46]

Validation using PROCHECK revealed that 81.1%, 76.7%, and 84.7% of residues in MEVPA, MEVPB, and MEVPC, respectively, were located within the most favored regions of the Ramachandran plot, with minimal residues in disallowed regions (Figure 4). Collectively, these results demonstrate that MEVP-C exhibited superior structural quality, as evidenced by its higher ERRAT score, more favorable Ramachandran distribution, and acceptable ProSA Z-score, underscoring its robustness for downstream vaccine applications.

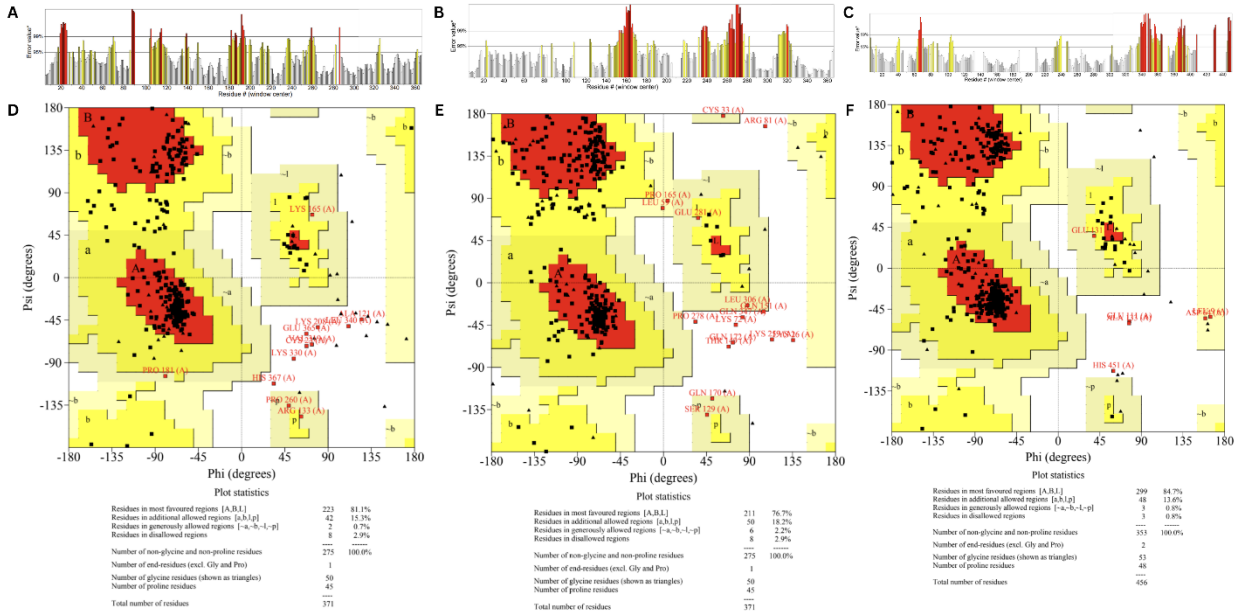


Figure 4. (A–C) ERRAT analysis of the MEVP constructs (MEVPA, MEVPB, and MEVPC), indicating overall model quality based on non-bonded atomic interactions; (D–F) Ramachandran plots of the respective constructs, illustrating the distribution of backbone dihedral angles and stereochemical quality.

Analysis of discontinuous B-cell epitope

The analysis of discontinuous B-cell epitopes within the 3D structures of the MEVPs was performed to characterize potential antibody-binding sites and their implications for immune recognition. Discontinuous epitopes, defined as conformational antigenic regions formed by spatially proximal amino acids, were predicted for each construct. A total of nine, seven, and ten discontinuous epitopes were identified in MEVPA, MEVPB, and MEVPC, respectively (Tables S6–S8; Figure 5). All predicted epitopes achieved scores above the threshold of 0.5, with the highest values being 0.827 for MEVPA, 0.968 for MEVPB, and 0.961 for MEVPC. The predicted epitope lengths ranged from 3–77 residues in MEVPA, 3–100 residues in MEVPB, and 3–83 residues in MEVPC. These findings suggest that all three constructs possess multiple conformational epitopes with strong antigenic potential, with MEVPB and MEVPC

displaying slightly higher maximum scores, indicative of potentially stronger antibody interactions.

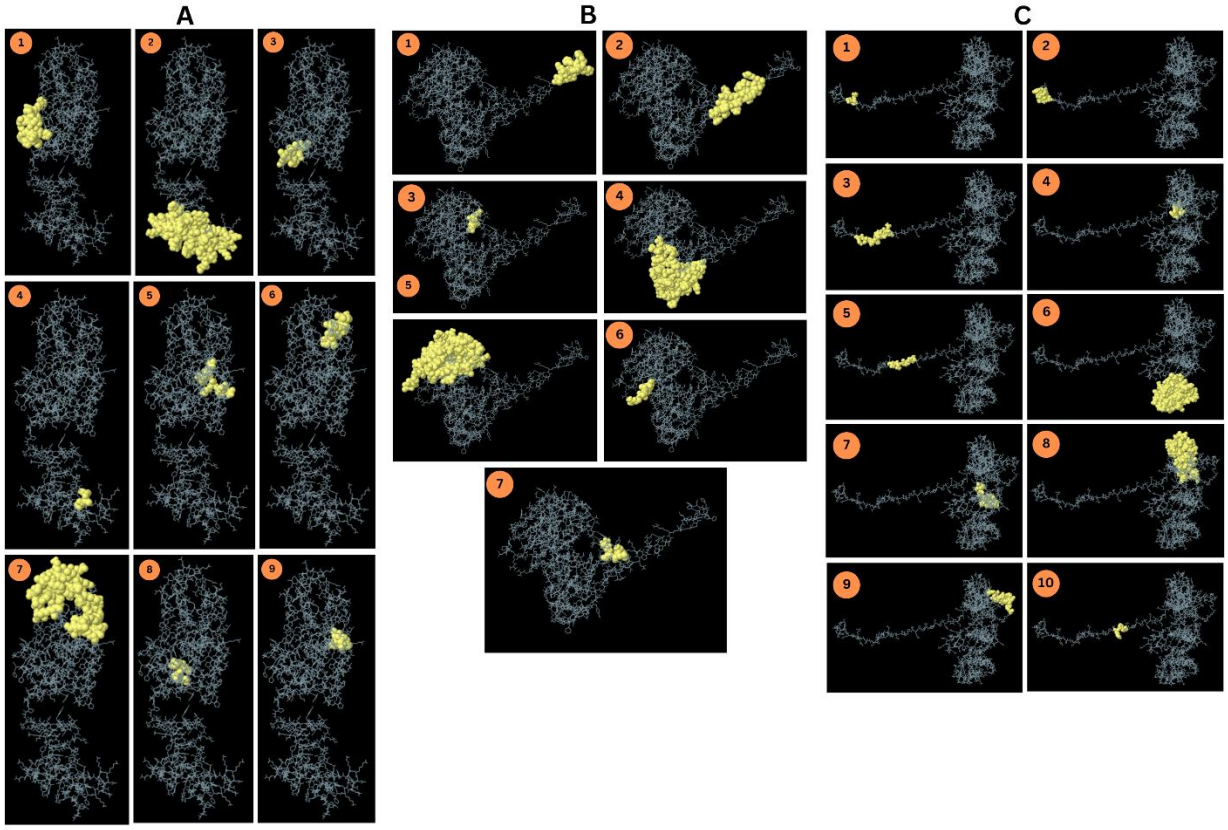


Figure 5. Predicted discontinuous B-cell epitopes in the 3D structures of MEVP-A, MEVP-B, and MEVP-C. Nine, seven, and ten conformational epitopes were identified, respectively, all with scores above 0.5.

Detection of potential disulfide engineering in MEVP

Disulfide engineering represents a rational protein design strategy to enhance structural stability and thermal resilience through the introduction of covalent disulfide bonds. In this study, the DbD2 server initially identified 21, 31, and 17 potential residue pairs in MEVPA, MEVPB, and MEVPC, respectively. These candidates were subsequently filtered based on stringent geometric criteria, including χ^3 dihedral angles within −87° to +97° (±30° tolerance) and a maximum Cα–Cβ–Sγ bond angle of 114.6°, to ensure conformational feasibility. Following this refinement, two residue pairs in MEVPA (LEU21–PHE71 and GLY293–ASP324), five pairs in MEVPB (PRO152–ALA243, ALA163–TYR186, GLY168–THR174, TYR176–TYR248, and SER299–SER302), and two pairs in MEVPC (LYS73–GLY76 and GLN448–HIS451) were identified as suitable candidates for cysteine substitution (Tables S9–S11). These selected pairs exhibit favorable geometric compatibility for disulfide bond formation, suggesting a high likelihood of successful covalent linkage without inducing structural strain.

Analysis of Active Sites in the MEVPs

Identifying protein active sites is a crucial step prior to molecular docking to accurately determine potential binding pockets using the PrankWeb server. The use of the PrankWeb server improves the reliability of active-site identification, as it integrates machine learning-based approaches for ligand-binding-site prediction. This approach

complements other prediction tools by providing consensus-based validation, thereby reducing false-positive predictions and enhancing the accuracy of selected binding residues for subsequent docking analysis.[47,48]

The top-ranked binding pocket of TLR9 showed the highest confidence with a score of 14.42 and a probability of 0.732, comprising 17 residues. Similarly, the primary pockets identified in MEVPA, MEVPB, and MEVPC exhibited favorable scores of 12.57, 12.78, and 13.73, with corresponding probabilities of 0.676, 0.684, and 0.713, respectively, and included 25, 21, and 29 residues. The distribution of these residues, as illustrated in Figure 6, indicates well-defined and surface-accessible regions, supporting their suitability as potential binding sites for subsequent molecular docking analysis.

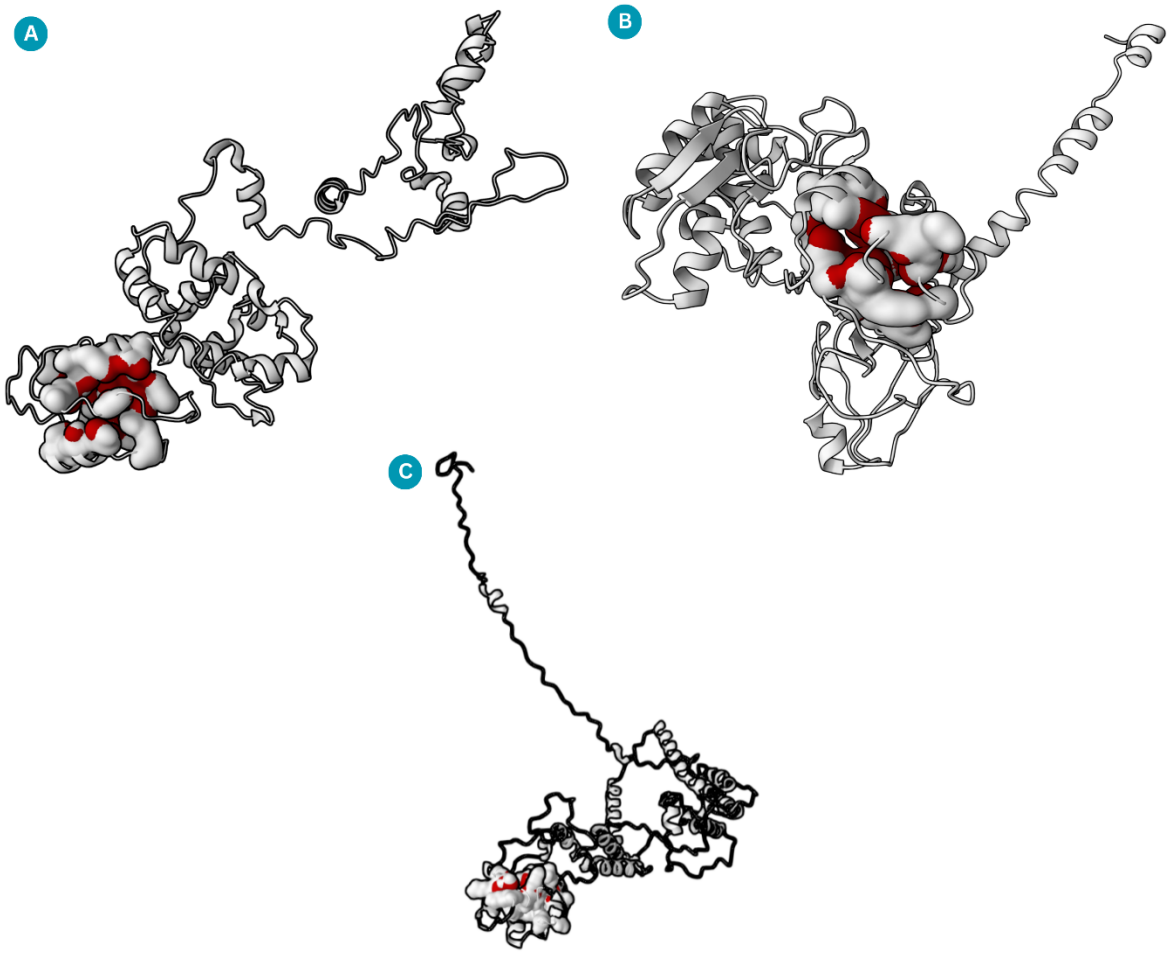


Figure 6. Predicted active binding sites in the MEVP constructs, highlighting the most probable ligand-binding pocket as a red sphere. Panels show (A) MEVPA, (B) MEVPB, and (C) MEVPC, indicating the location of the dominant binding region in each structure.

Docking Simulation and Interaction Analysis of MEVP–TLR9 Complexes

Molecular docking was performed to evaluate the interactions between the multi-epitope vaccine peptides (MEVPs) and TLR9, as well as to determine their optimal binding conformations. Docking analysis using HADDOCK 2.4 revealed that MEVPC exhibited the most favorable interaction, as indicated by the lowest HADDOCK score (−131.5 ± 2.0), compared to MEVPA (−119.2 ± 3.5) and MEVPB (−99.7 ± 0.6), suggesting stronger binding affinity. This

result is further supported by its more favorable van der Waals (−75.5 ± 2.2) and desolvation energy (−21.9 ± 2.1), along with a relatively large buried surface area (2186.2 ± 64.8), indicating stable complex formation. In contrast, MEVPA showed the most favorable binding free energy based on PRODIGY analysis (ΔG = −10.9 kcal/mol; Kd = 1 × 10^{-8} M), followed by MEVPC and MEVPB. Interaction profiling using PDBsum demonstrated that all complexes were stabilized by a combination of non-covalent interactions, including hydrogen bonds, salt bridges, and non-bonded contacts, with MEVPB showing the highest number of hydrogen bonds (11) and non-bonded contacts (86), while MEVPC formed the highest number of salt bridges (3) (Figure 7). Overall, despite slight variations across parameters, MEVPC consistently demonstrated a favorable binding profile, supporting its potential to enhance receptor recognition and subsequent immune activation.

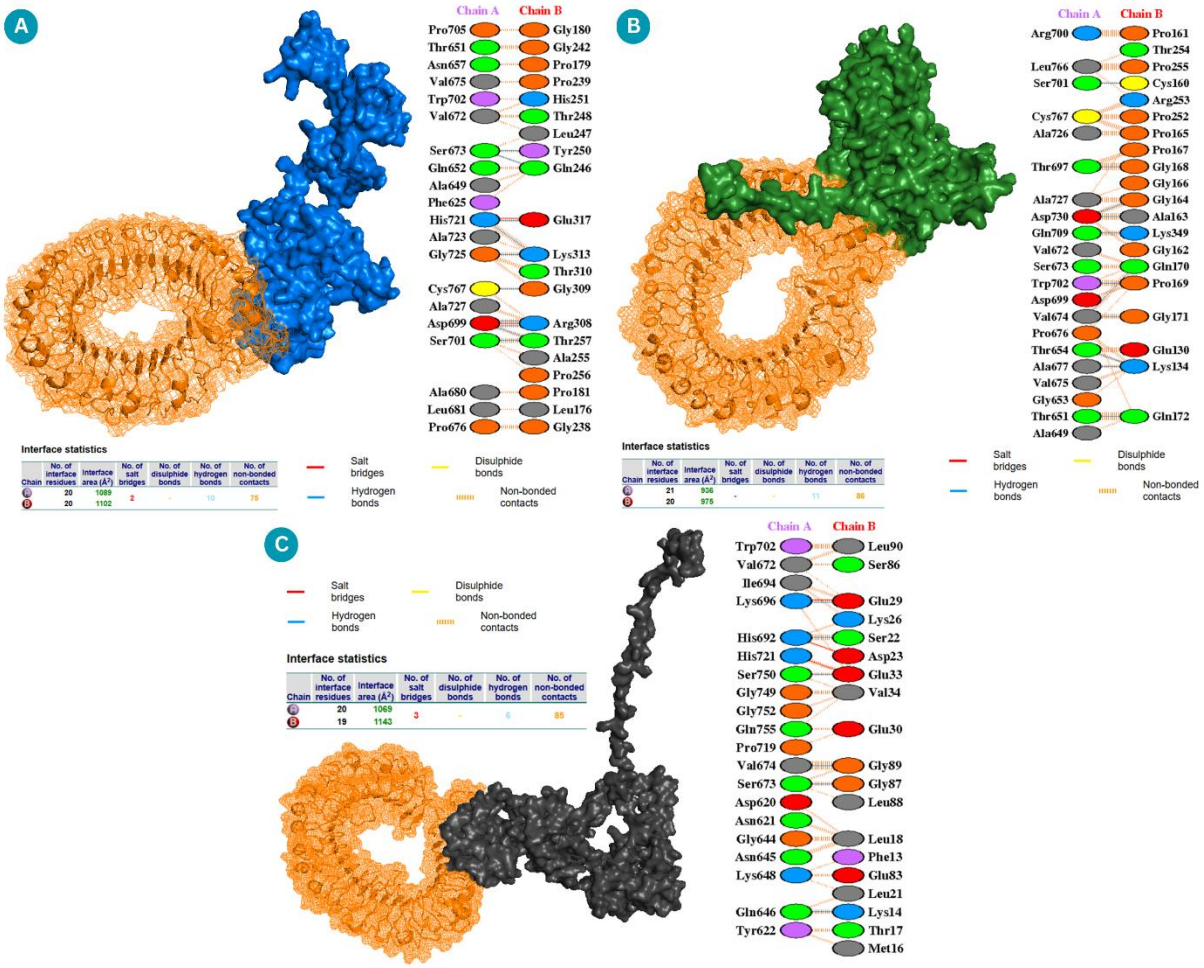


Figure 7. Molecular docking of Toll-like receptor 9 (TLR9) with the MEVP constructs, showing binding conformations, interacting residues, and interface interaction profiles. (A) TLR9–MEVPA, (B) TLR9–MEVPB, and (C) TLR9–MEVPC. Docking was performed using HADDOCK 2.4 and the refinement complexes were visualized with PDBsum.

Table 2. Result of docking of MEVPs with TLR9

Docking Tools	Parameters	MEVPA	MEVPB	MEVPC
HADDOCK2.4	HADDOCK score	-119.2 ± 3.5	-99.7 ± 0.6	-131.5 ± 2.0
	Cluster size	20	20	20
	RMSD from the overall lowest-energy structure	0.7 ± 0.4	0.7 ± 0.4	0.7 ± 0.4
	Van der Waals energy	-70.3 ± 1.3	-71.1 ± 2.0	-75.5 ± 2.2
	Electrostatic energy	-192.9 ± 27.9	-151.0 ± 5.8	-171.0 ± 9.2
	Desolvation energy	-10.4 ± 2.1	1.5 ± 1.1	-21.9 ± 2.1
	Restraints violation energy	1.1 ± 0.4	1.0 ± 0.2	0.9 ± 0.1
	Buried Surface Area	2222.4 ± 39.4	2002.6 ± 25.9	2186.2 ± 64.8
	Z-Score	0.0	0.0	0.0
PRODIGY	ΔG(kcal/mol)	-10.9	-9.4	-9.6
	Kd (M) at 25.0°C	1e-08	1.2e-07	8.7e-08
PDBsum	Number of Hydrogen Bonds	10	11	6
	Number of Salt Bridges	2		3
	Number of Non-Bounded Contacts	75	86	85

Molecular dynamics and MMGBSA of MEVP and human toll-like receptor 9 (TLR-9)

Molecular dynamics show that the backbone RMSD profile illustrates the stability dynamics of the three protein–protein complexes over a 100 ns simulation period. RMSD values were employed to assess conformational deviations relative to the initial structure. The MEVPA–TLR9 system (blue line) demonstrated relatively stable behavior, maintaining RMSD values within ~1.0–1.4 nm. Following an initial equilibration phase, the system reached a steady state with minimal fluctuations, indicating that intermolecular interactions remained well preserved throughout the simulation. In contrast, the MEVPB–TLR9 system (green line) exhibited low RMSD values (~0.8–1.0 nm) during the early to mid-stages of the simulation, suggesting structural stability; however, a marked increase in RMSD was observed toward the end (~100 ns), consistent with trajectory visualization showing progressive separation of the two proteins, indicative of late-stage dissociation. Conversely, the MEVPC–TLR9 system (red line) displayed the highest RMSD values (~2.2 nm), accompanied by pronounced spikes reaching nearly 5 nm between 60–80 ns. These fluctuations reflect substantial conformational rearrangements which, based on trajectory analysis, correspond to dissociation events, highlighting the pronounced instability of this complex. The average RMSD values further support these observations, with MEVPB–TLR9 at ~0.916 nm, MEVPA–TLR9 at ~1.206 nm, and MEVPC–TLR9 at ~2.218 nm. Collectively, although MEVPB–TLR9 appeared stable in the initial phase, it failed to maintain structural integrity toward the end of the simulation. MEVPA–TLR9 emerged as the most stable system overall, whereas MEVPC–TLR9 exhibited the lowest stability, with early and significant dissociation events (Figure 8A).

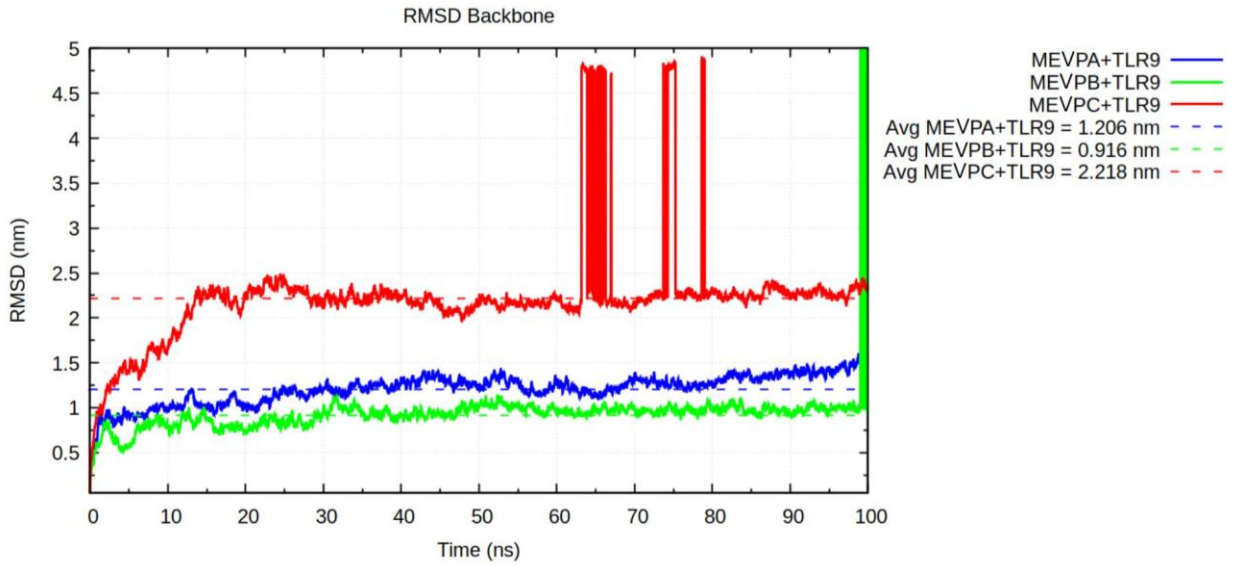


Figure 8A. Backbone RMSD of MEVPA–TLR9 (blue), MEVPB–TLR9 (green), and MEVPC–TLR9 (red) over 100 ns. MEVPA–TLR9 shows the greatest stability, MEVPB–TLR9 is stable early but dissociates near 100 ns, while MEVPC–TLR9 exhibits high fluctuations with spikes at 60–80 ns, indicating protein separation.

Conversely, the number of protein–protein hydrogen bonds (H-bonds) over the 100 ns simulation indicates that the MEVPC–TLR9 complex exhibits the highest average (~686.6), followed by MEVPA–TLR9 (~628.7) and MEVPB–TLR9 (~619.9). However, the elevated H-bond count in MEVPC–TLR9 does not translate into structural stability, as substantial fluctuations suggest highly dynamic and unstable interactions, consistent with RMSD results indicating dissociation. In contrast, MEVPA–TLR9 maintains a moderate yet stable H-bond profile, reflecting more consistent interactions that support overall complex stability. Meanwhile, MEVPB–TLR9 shows the lowest H-bond count and a weakening interaction pattern toward the end of the simulation, correlating with dissociation events near 100 ns. Overall, these findings highlight that complex stability is governed not only by the number of H-bonds but also by their persistence and dynamic behavior throughout the simulation (Figure 8B).

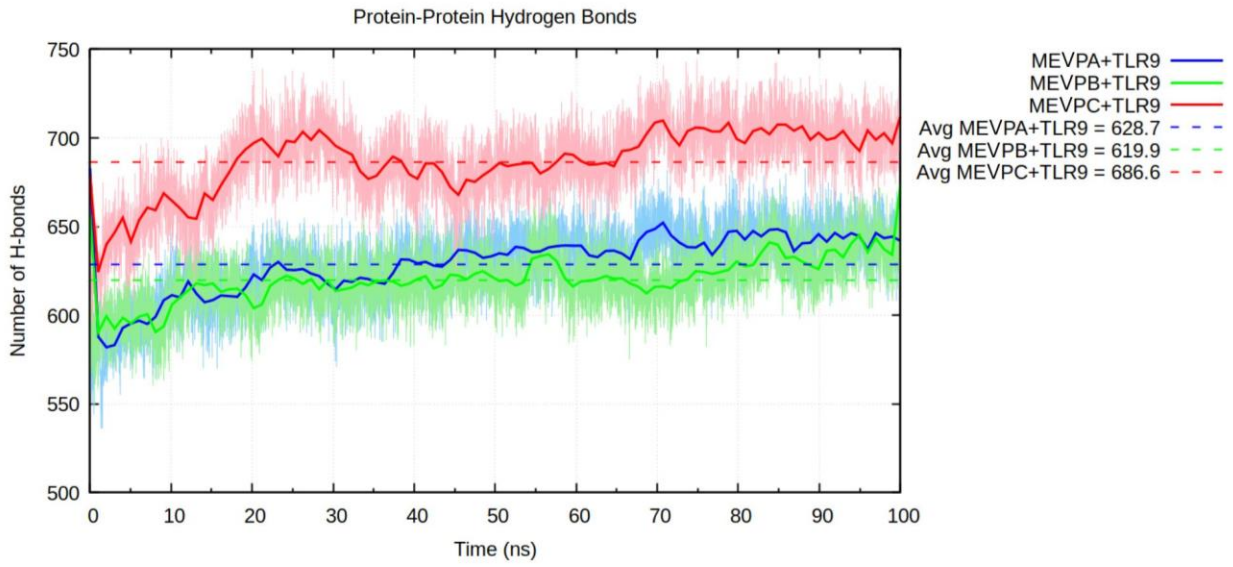


Figure 8B. Protein–protein hydrogen bonds (H-bonds) in the MEVPA–TLR9 (blue), MEVPB–TLR9 (green), and MEVPC–TLR9 (red) complexes over 100 ns. MEVPC–TLR9 shows the highest number of H-bonds, followed by MEVPA–TLR9 and MEVPB–TLR9.

SASA analysis was performed to evaluate the solvent-accessible surface area of the protein complexes, where an increase in SASA reflects relative structural expansion.[49] The SASA profiles over the 100 ns simulation reveal dynamic changes in solvent exposure among the systems. The MEVPC–TLR9 complex (red) exhibits the highest SASA value (~578.0 nm²), indicating greater surface exposure, consistent with its lower stability and dissociation tendency observed in the RMSD analysis. In contrast, MEVPB–TLR9 (green) shows the lowest SASA (~526.3 nm²), suggesting a more compact structure for most of the simulation, although signs of dissociation emerge toward the end. The MEVPA–TLR9 system (blue) displays intermediate SASA values (~541.3 nm²) with moderate fluctuations, reflecting a balance between structural flexibility and stability. Overall, an initial decrease in SASA followed by a plateau suggests structural adaptation toward a more stable conformational state (Figure 8C).

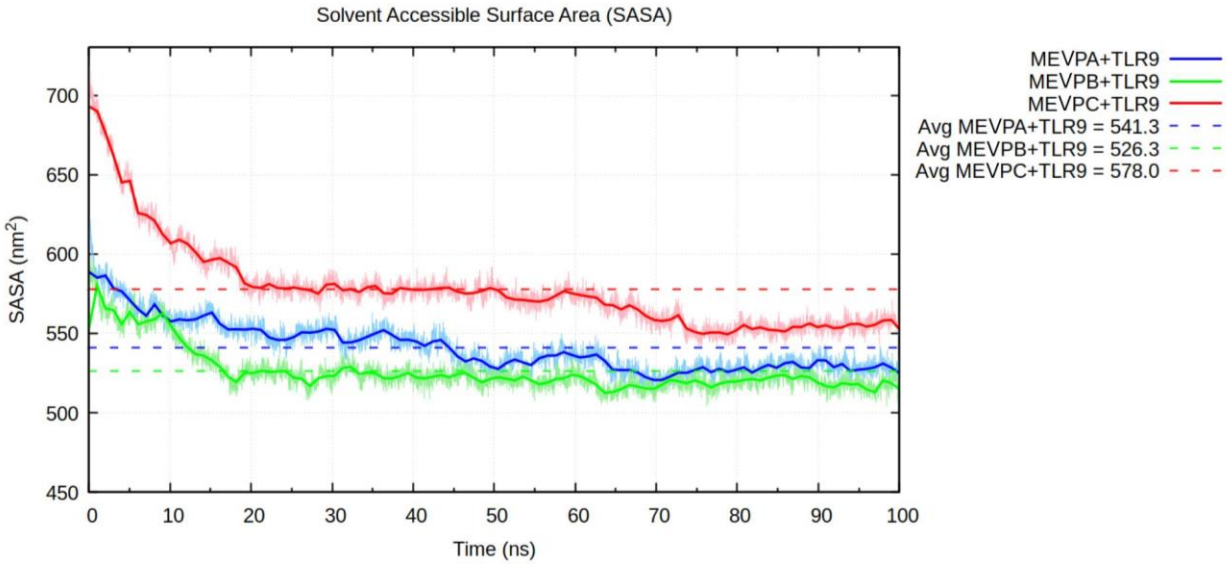


Figure 8C. Solvent-accessible surface area (SASA) of the MEVPA–TLR9 (blue), MEVPB–TLR9 (green), and MEVPC–TLR9 (red) complexes over 100 ns. MEVPC–TLR9 shows the highest SASA (greater exposure), whereas MEVPB–TLR9 is the most compact; MEVPA–TLR9 exhibits relatively stable behavior with moderate fluctuations.

Overall, the combined analyses of RMSD, hydrogen bonds (H-bonds), and solvent-accessible surface area (SASA) reveal marked differences in stability among the three protein–protein complexes. The MEVPA–TLR9 system exhibits the highest stability, characterized by relatively low and stable RMSD values, supported by a moderate number of H-bonds and moderate SASA fluctuations, reflecting a balance between structural flexibility and compactness. The MEVPB–TLR9 complex initially appears stable, with low RMSD and a compact structure (low SASA), but undergoes dissociation toward the end of the simulation, indicating that intermolecular interactions are insufficient to maintain long-term stability. In contrast, the MEVPC–TLR9 system shows the lowest stability, as evidenced by high RMSD values and pronounced spikes associated with protein separation, despite having the highest number of H-bonds and the largest SASA. This finding highlights that a higher number of interactions does not necessarily correlate with greater stability; rather, the consistency and dynamic behavior of these interactions are more critical. Collectively, MEVPA–TLR9 emerges as the most stable complex, followed by MEVPB–TLR9, while MEVPC–TLR9 is comparatively unstable and prone to dissociation during the simulation.

Furthermore, the binding affinity of the MEVP–TLR9 complexes was evaluated using molecular mechanics/generalized Born surface area (MM-GBSA) calculations via the HawkDock server. As presented in Table 3, MEVP-A exhibited the most favorable total binding free energy (−62.15 kcal/mol), followed by MEVPC (−49.10 kcal/mol) and MEV-B (−30.33 kcal/mol). The strong binding of MEVPA is primarily driven by balanced van der Waals (−109.18 kcal/mol) and solvation contributions (GB: −1144.38 kcal/mol; SA: −14.42 kcal/mol), which effectively offset the electrostatic component. In contrast, although MEVP-B showed a high electrostatic contribution (1640.6 kcal/mol), it was counteracted by unfavorable overall energy, while MEVPC displayed moderate contributions across all components. These findings indicate that MEVPA forms the most stable complex with TLR9, highlighting its potential as a promising vaccine candidate for further development.

Table 3. MM/GBSA binding free energy of MEVP-TLR9 complex calculated using Hawkdock.

Parameters	MEVP-A	MEVP-B	MEVP-C
Van der Waals	-109.18	-99.37	-110.84
Electrostatic energy	1205.82	1640.6	-145.56
Generalized Born	-1144.38	-1558.87	221.25
Surface Area	-14.42	-12.7	-13.96
Total (kcal/mol)	-62.15	-30.33	-49.1

Codon Optimization and In Silico Cloning of MEVP Constructs

To enhance the expression of the MEVP sequence in a heterologous host, codon adaptation was performed to reverse-translate the amino acid sequence into nucleotide sequences using the JCat server. The optimized cDNA sequences for constructs A and B consisted of 1,113 nucleotides each, with a GC content of 57.68%, while construct C consisted of 1,118 nucleotides with a GC content of 55.77%. All constructs exhibited GC content within the optimal range of 40–60%, indicating suitability for efficient transcription and translation in the chosen expression system.

The codon adaptation index (CAI) for all constructs was 1.0, which falls within the ideal range of 0.8–1.0, suggesting high compatibility of the codon usage with the host organism and predicting maximal translational efficiency. For downstream cloning purposes, the sequences were flanked with buffer-compatible restriction sites, with BamHI at the 5′ end and EcoRI at the 3′ end, allowing seamless insertion into the expression vector. The in-silico cloning analysis illustrated the codon sequences in red and the vector backbone in black, resulting in a final recombinant plasmid length of 6,480 bp for MEVPA and MEVPB and 6,735 bp for construct MEVPC (Figure 9). These findings indicate that the constructs are well-optimized for high-level expression and are ready for subsequent experimental validation.

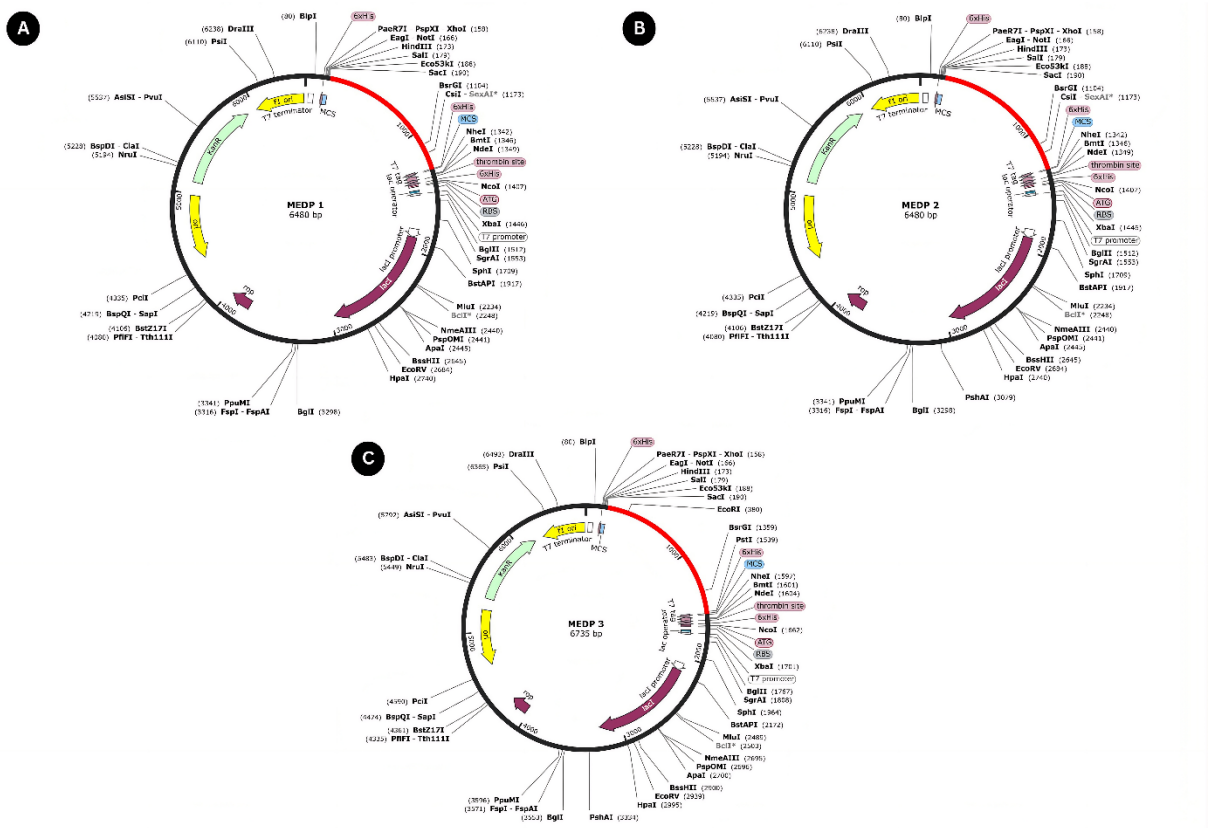


Figure 9. In silico cloning of MEVPs into the pET28a(+) expression vector. The codon-optimized gene sequences were inserted into the vector, with the cloned regions highlighted in red. (A) MEVP-A, (B) MEVP-B, and (C) MEVP-C.

Immune Simulation

Immune simulations following three administrations of MEVPC, one of the best constructs, on days 0, 28, and 56 predicted robust activation of both the innate and adaptive immune compartments. Natural killer (NK) cells remained stable with minor fluctuations throughout the 350-day period (Figure A), while dendritic cells (DCs) and macrophages (MAs) displayed dynamic changes, reflecting effective antigen uptake and presentation, with peak activation occurring shortly after each injection (Figures 10B and 10C). Antigen-specific antibody responses, including IgM, IgG1, and IgG2, significantly increased after each booster, with IgG1 and IgG2 persisting at high levels throughout the observation period, indicating successful humoral memory formation (Figure 10D). Correspondingly, key cytokines such as IFN-γ and IL-4 exhibited sharp peaks after each immunization, supporting robust Th1/Th2 polarization (Figure 10E).

Cellular immune responses were also enhanced, as shown by increases in total and memory T-helper (TH) and cytotoxic T (TC) cell populations following vaccination, with memory cells gradually stabilizing after the final booster (Figures 10F and 10G). Plasma B cells (PLBs) displayed transient expansion correlating with antibody peaks (Figure 10H), while total and memory B-cell populations demonstrated sustained activation and differentiation (Figure 10I), reflecting effective induction of long-term humoral immunity. Collectively, these simulations suggest that the EBV multiepitope vaccine can elicit coordinated innate and adaptive immune responses, including strong cytokine

production, antibody generation, and memory T/B-cell formation, supporting its potential for long-lasting protective immunity.

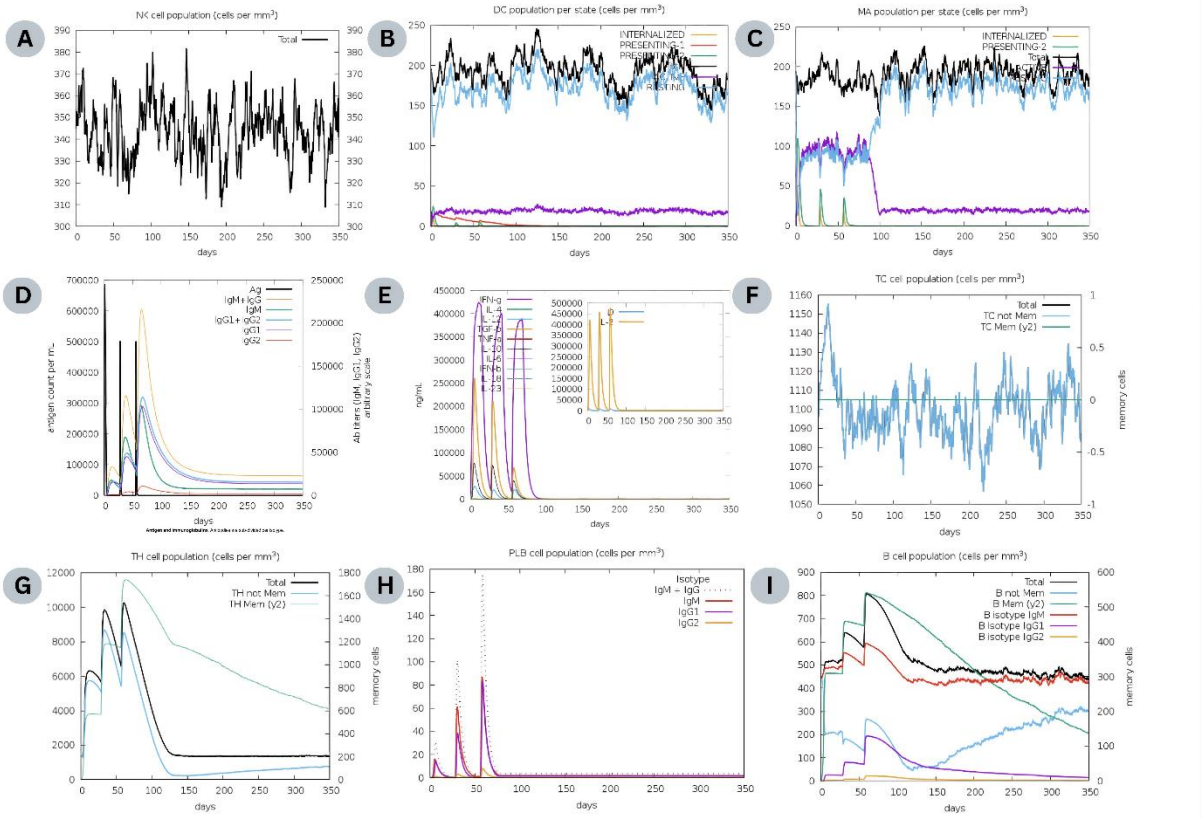


Figure 10. Immune simulation of MEVPC with three injection. (A) Natural Killer cells total count (B) Dendritic cells total count (C) Macrophage total count (D) Antigen and immunoglobulins. Antibodies are sub-divided per isotype (E) Cytokines release (F) CD8 T-cytotoxic lymphocytes count (G) CD4 T-helper lymphocytes count (H) Plasma B lymphocytes count sub-divided per isotype (IgM, IgG1 and IgG2) (I) B lymphocytes: total count, memory cells, and sub-divided in isotypes IgM, IgG1 and IgG2.

Discussion

Gastric cancer (GC) remains one of the leading causes of cancer-related mortality worldwide, with multiple risk factors contributing to its development. Among its subtypes, Epstein-Barr virus-associated gastric cancer (EBVaGC) represents approximately 9% of global GC cases and exhibits distinct clinicopathological features. EBVaGC is more prevalent in males, often occurs in the proximal region of the stomach, and demonstrates a lymphoepithelioma-like histological pattern. Moreover, this subtype is characterized by unique molecular profiles, including frequent mutations in genes, widespread DNA hypermethylation, and activation of immune-related signaling pathways.[1,50]

Epstein-Barr virus (EBV) contributes to gastric cancer through several mechanisms, including direct infection of gastric epithelial cells and modulation of the tumor microenvironment. EBV can infect gastric epithelial

cells via interactions with ephrin receptors and integrins, leading to viral replication and oncogenic transformation. Additionally, EBV infection induces DNA hypermethylation and activation of immune signaling pathways, such as the PI3K/AKT pathway, promoting tumorigenesis in gastric cells.[3,51] These molecular alterations characterize EBV-associated gastric cancer (EBVaGC) as a distinct subtype with unique genetic and epigenetic features.[1]

Current therapeutic strategies encompass adoptive cellular therapies, such as EBV-specific cytotoxic T lymphocyte (EBV-CTL) infusions, which have demonstrated safety and efficacy in treating EBV-associated lymphomas and PTLD.[52,53] Additionally, monoclonal antibodies targeting CD20, like rituximab, are utilized in managing EBV-positive malignancies; however, resistance and relapse remain concerns.[54] The development of vaccines targeting EBV antigens, particularly those expressed during latency, is a promising avenue for both therapeutic and preventive measures. Recent advancements include the design of multi-epitope vaccines that incorporate both structural and non-structural EBV proteins, aiming to elicit robust T-cell and antibody responses.[55] For instance, a study by Dasari et al. (2023) developed a lymph node-targeted multi-epitope subunit vaccine that effectively promoted immunity against EBV in HLA-expressing mice.[56] These innovative approaches hold promise for enhancing immune surveillance and preventing the onset of EBV-associated cancers. In this study, we designed an immunodominant multiepitope-based vaccine aimed at both preventing and treating EBV-associated gastric cancer (EBVaGC), focusing on two critical proteins, BZLF1 and EBNA1. These proteins play essential roles in EBV infection and tumorigenesis, making them promising targets for eliciting robust immune responses and controlling EBV-driven malignancies.

At the initial stage of construct design, we performed T- and B-cell epitope prediction and ensured that the selected epitopes were antigenic, non-allergenic, and non-toxic. The identification and characterization of T- and B-cell epitopes represent fundamental steps in vaccine development, as T-cell epitopes presented by MHC class I and II molecules initiate cellular immunity, while B-cell epitopes are recognized by antibodies to induce humoral responses. This is further supported by the population coverage analysis, which demonstrated a high global coverage of 97.25%, indicating that the selected epitopes are broadly representative across diverse populations. Computational immunoinformatics enables precise selection of antigenic regions most likely to be recognized by the host immune system, thereby enhancing the safety, specificity, and overall effectiveness of the proposed vaccine.[13,57] Furthermore, ensuring that predicted epitopes are non-allergenic and non-toxic is critical to minimize adverse reactions during in vitro and in vivo applications, thereby improving the safety profile of vaccine. This integrative approach facilitates the rational design of effective vaccine by focusing on immunodominant epitopes contributing to the accurate stimulate immune response.[58]

In this vaccine construct, two different adjuvants were employed, and the arrangement of epitopes was optimized to generate a candidate with favorable characteristics and the ability to induce strong immune responses in silico. Among the designed constructs, MEVPC demonstrated the most promising profile, being immunogenic and non-toxic. This construct incorporates the ribosomal protein L7/L12 as well as a TLR9 agonist adjuvant, which effectively activates dendritic cells, thereby promoting naïve T-cell activation, $CD4^+$ and $CD8^+$ T-cell differentiation, and T cell–mediated cytotoxicity. Given the critical role of TLR9 in EBV infection and host immune regulation, its engagement in this construct underscores the potential of MEVPC as a strong prophylactic and therapeutic vaccine candidate against EBV-associated diseases.[59,60]

The designed multiepitope vaccine construct had a molecular weight of 46,807.28 Da, which is within the favorable range for recombinant protein expression and purification. Proteins with molecular weights below 100 kDa are generally considered suitable for large-scale production, stability, and immunogenicity in recombinant vaccine development. In addition, the ERRAT quality factor of 75 indicates that the model has acceptable non-bonded atomic interactions, as scores above 50 are typically considered reliable for structural validation.[43,46]

Furthermore, structural validation using the Ramachandran plot showed that 84.7% of residues were located in the most favored regions, suggesting a stable and stereochemically reliable conformation of the modelled vaccine. The ProSA Z-score of –3.33 also falls within the range of native proteins of similar size, further supporting the overall quality and reliability of the vaccine construct. These validation results collectively indicate that the designed multiepitope vaccine is structurally sound and suitable for downstream immunological evaluation.

Molecular docking results show that all three constructed vaccines can bind to TLR9. Toll-like receptor 9 (TLR9) plays a crucial role in antiviral immunity by recognizing unmethylated CpG motifs commonly found in viral DNA, including Epstein-Barr virus (EBV). Engagement of TLR9 activates downstream signaling pathways that induce type I interferons and pro-inflammatory cytokines, thereby bridging innate and adaptive immune responses. In the context of EBV-associated malignancies, activation of TLR9 enhances antigen presentation and promotes robust T-cell mediated responses, which are essential for controlling latent and lytic EBV infections.[61,62]

Incorporating TLR9 engagement into EBV vaccine design is particularly important for inducing strong immunogenicity and breaking viral immune evasion strategies. TLR9 agonists have been shown to act as potent adjuvants that amplify both humoral and cellular immune responses, making them attractive candidates for therapeutic and preventive EBV vaccines. Specifically, triggering TLR9 can enhance recognition of EBV latent antigens such as EBNA1 and lytic antigens like BZLF1, improving vaccine efficacy against EBV-associated cancers. Therefore, targeting TLR9 signalling represents a promising strategy to develop next-generation EBV vaccines with enhanced immunostimulatory potential.[9,63–65]

The results of the vaccine, especially the C construct, appear to trigger cellular and humoral immune responses, including innate immunity. The immune simulation results provide compelling evidence that the designed EBV multiepitope vaccine construct has the potential to induce strong and durable protective immunity. The robust activation of both innate and adaptive compartments, characterized by dynamic responses of dendritic cells and macrophages, suggests effective antigen processing and presentation, which are crucial for initiating downstream adaptive responses. The persistence of IgG1 and IgG2, together with the expansion of plasma B cells and sustained memory B-cell populations, indicates the induction of long-lasting humoral immunity, an essential feature for preventing EBV reactivation and associated malignancies. [66–68]

Moreover, the simultaneous enhancement of Th1- and Th2-associated cytokines, particularly IFN-γ and IL-4, highlights balanced immune polarization, which is advantageous for combating EBV infections that involve both latent and lytic phases. The expansion and stabilization of memory T-helper and cytotoxic T-cell populations further underscore the construct's capacity to establish long-term immunological memory, a critical requirement for therapeutic efficacy against EBV-associated cancers such as EBV-positive gastric carcinoma and nasopharyngeal carcinoma. Collectively, these findings support the potential of the multiepitope vaccine as a promising candidate for both prophylactic and therapeutic applications against EBV-associated diseases.[57]

Despite these promising findings, the results of this study remain limited to in silico predictions and thus require further validation through in vitro and in vivo experiments. Computational approaches such as epitope prediction, molecular docking, and immune simulations provide valuable insights into vaccine design; however, they cannot fully capture the complexity of host–pathogen interactions, immune regulation, and potential off-target effects in biological systems. Therefore, experimental studies are essential to confirm antigen processing, epitope presentation, immunogenicity, and safety of the proposed EBV multiepitope vaccine.

Future research should focus on expressing and purifying the designed construct in suitable expression systems, followed by immunological assays in cell culture and preclinical animal models to validate the predicted immune responses. Such experimental validation is particularly crucial for EBV vaccines, as the virus exhibits complex latency programs and immune evasion strategies that may alter vaccine performance in vivo. Thus, while in silico design provides a strong foundation, translational research bridging computational and experimental studies is indispensable for advancing EBV vaccine candidates toward clinical application.

Conclusion

In summary, all designed multiepitope vaccine constructs (MEVPs) exhibited favorable immunological properties, including antigenicity, non-allergenicity, and non-toxicity. Although MEVPC demonstrated superior physicochemical properties and the most favorable docking score toward TLR9, further binding energy analyses and molecular dynamics simulations revealed that the MEVPA–TLR9 complex possesses the highest binding affinity and structural stability. In contrast, MEVPC showed lower stability despite its strong initial interaction profile. Notably, immune simulation results indicated that MEVPC induced robust and sustained immune responses, including strong antibody production and memory cell formation. Despite these promising in silico findings, experimental validation remains essential to advance these candidates toward clinical application. Future studies should include in vitro and in vivo evaluations to confirm immunogenicity, safety, and protective efficacy against EBV-associated gastric cancer.

Acknowledgments

Gratefully thank to Faculty of Medicine Uiversitas Palangka Raya, Faculty of Medicine and Institute of Research and Community Service, Ahmad Dahlan University

Author Contributions

Rachma Greta Perdana Putri: Investigation, Formal Analysis, Resources, Funding Acquisition. Ysrafil Ysrafil: Data curation, Software, Supervision, Visualization. Leonny Dwi Rizkita: Conceptualization, Formal analysis. Annisa: Investigation, Writing - Original Draft, Formal Analysis. Barkah Djaka Purwanta: Supervision, Writing - Review & Editing., Project administration.

Ethics

Not Applicable

Conflict of Interest

On behalf of all authors, the corresponding author states that there is no conflict of interest

Funding

The authors extend their thanks to the Institute of Research and Community Service, Ahmad Dahlan University for funding this research (PD-101/SP3/LPPM-UAD/VIII/2023).

Data Availability

Data will be made available on request.

References

1. Corallo S, Lasagna A, Filippi B, Alaimo D, Tortorella A, Serra F, et al. Unlocking the Potential: Epstein-Barr Virus (EBV) in Gastric Cancer and Future Treatment Prospects, a Literature Review. Pathogens. 2024;13:1-17. doi: 10.3390/pathogens13090728.
2. Hirabayashi M, Georges D, Clifford GM, de Martel C. Estimating the Global Burden of Epstein-Barr Virus-Associated Gastric Cancer: A Systematic Review and Meta-Analysis. Clin Gastroenterol Hepatol. 2023;21(4): 922–30. doi: 10.1016/j.cgh.2022.07.042.
3. Salnikov MY, MacNeil KM, Mymryk JS. The viral etiology of EBV-associated gastric cancers contributes to their unique pathology, clinical outcomes, treatment responses and immune landscape. Front Immunol. 2024;15:1358511. doi: 10.3389/fimmu.2024.1358511.
4. Soldan SS, Messick TE, Lieberman PM. Therapeutic approaches to Epstein–Barr virus cancers. Curr Opin Virol. 2022;52:101260. doi: 10.1016/j.coviro.2022.101260.
5. Cohen JI, Fauci AS, Varmus H, Nabel GJ. Epstein-Barr virus: An important vaccine target for cancer prevention. Sci Transl Med. 2011;3(107):107ps7. doi: 10.1126/scitranslmed.3002878.
6. Tan H, Gong Y, Liu Y, Long J, Luo Q, Faleti OD, et al. Advancing therapeutic strategies for Epstein-Barr virus-associated malignancies through lytic reactivation. Biomed Pharmacother. 2023;164(August 2023):114916. doi: 10.1016/j.biopha.2023.114916.
7. Li P, Meng Z, Zhou Z, Zhong Z, Kang M. Therapeutic vaccines for Epstein–Barr virus: a way forward. Lancet. 2024;403(10446):2779–80. doi: 10.1101/2024.04.12.24305195.
8. Silveira ELV, Fogg MH, Leskowitz RM, Ertl HC, Wiseman RW, O'Connor DH, et al. Therapeutic vaccination against the rhesus lymphocryptovirus EBNA-1 homologue, rhEBNA-1, elicits T cell responses to novel epitopes in rhesus macaques. J Virol. 2013;87(24):13904–10. doi: 10.1128/jvi.01947-13.
9. Hartlage AS, Liu T, Patton JT, Garman SL, Zhang X, Kurt H, et al. The Epstein-Barr virus lytic protein BZLF1 as a candidate target antigen for vaccine development. Cancer Immunol Res. 2015;3(7):727–94. doi: 10.1158/2326-6066.CIR-14-0242.
10. Ysrafil Y, Imran AK, Wicita PS, Kamba V, Mohamad F, Ismail I, et al. Mosaic vaccine design targeting mutational spike protein of SARS-CoV-2: An immunoinformatics approach. BioImpacts. 2025;15:26443. doi: 10.34172/bi.2023.26443.
11. Safavi A, Kefayat A, Sotoodehnejadnematalahi F, Salehi M, Modarressi MH. Production, purification, and in vivo evaluation of a novel multiepitope peptide vaccine consisted of immunodominant epitopes of SYCP1 and ACRBP antigens as a prophylactic melanoma vaccine. Int Immunopharmacol. 2019;76(2019):105872. doi: 10.1016/j.intimp.2019.105872.
12. Qiu J, Wei Y, Shu J, Zheng W, Zhang Y, Xie J, et al. Integrated in-silico design and in vivo validation of multi-epitope vaccines for norovirus. Virol J. 2025;22(1):166. doi: 10.1186/s12985-025-02796-6.
13. Doytchinova IA, Flower DR. VaxiJen: A server for prediction of protective antigens, tumour antigens and subunit vaccines. BMC Bioinformatics. 2007;8:4. doi: 10.1186/1471-2105-8-4.

14. Dimitrov I, Flower DR, Doytchinova I. AllerTOP - a server for in silico prediction of allergens. BMC Bioinformatics. 2013;14(Suppl 6):S4. doi: 10.1186/1471-2105-14-S6-S4.
15. Gupta S, Kapoor P, Chaudhary K, Gautam A, Kumar R, Raghava GPS. In silico approach for predicting toxicity of peptides and proteins. PLoS One. 2013;8(9):e73957. doi: 10.1371/journal.pone.0073957.
16. Nugraha MF, Changestu DA, Ramadhan R, Salsabila T, Nurizati A, Pratiwi SE, et al. Novel prophylactic and therapeutic multi-epitope vaccine based on Ag85A, Ag85B, ESAT-6, and CFP-10 of Mycobacterium tuberculosis using an immunoinformatics approach. Osong Public Health Res Perspect. 2024;15(4):286–306. doi: 10.24171/j.phrp.2024.0026.
17. Pratiwi SE, Ysrafil Y, Mardhia M, Mahyarudin M, Ilmiawan MI, Trianto HF, et al. A novel therapeutic multiepitope vaccine based on oncoprotein E6 and E7 of HPV 16 and 18: An in silico approach. BioImpacts. 2024;14(5):27846. doi: 10.34172/bi.2024.27846.
18. Hossain MS, Hossan MI, Mizan S, Moin AT, Yasmin F, Akash AS, et al. Immunoinformatics approach to designing a multi-epitope vaccine against Saint Louis encephalitis virus. Inform Med Unlocked. 2021;22(2021):100500. doi: 10.1016/j.imu.2020.100500.
19. Ysrafil Y, Sapiun Z, Astuti I, Anasiru MA, Slamet NS, Hartati H, et al. Designing multi-epitope based peptide vaccine candidates against SARS-CoV-2 using immunoinformatics approach. BioImpacts. 2022;12(4):359-70. doi: 10.34172/bi.2022.23769.
20. Ryan N, Pratiwi SE, Mardhia M, Ysrafil Y, Liana DF, Mahyarudin M. Immunoinformatics approach for design novel multiepitope prophylactic and therapeutic vaccine based on capsid proteins L1 and L2 and oncoproteins E6 and E7 of human papillomavirus 16 and human papillomavirus 18 against cervical cancer. Osong Public Health Res Perspect. 2024;15(4):307-28. doi: 10.24171/j.phrp.2024.0013.
21. Shabbir MA, Amin A, Hasnain A, Shakeel A, Gul A. Immunoinformatics-driven design of a multi-epitope vaccine against Nipah virus: A promising approach for global health protection. J Genet Eng Biotechnol. 2025; 23(2):100482. doi: 10.1016/j.jgeb.2025.100482.
22. Gasteiger E, Gattiker A, Hoogland C, Ivanyi I, Appel RD, Bairoch A. ExPASy: The proteomics server for in-depth protein knowledge and analysis. Nucleic Acids Res. 2003;31(13):3784-8. doi: 10.1093/nar/gkg563.
23. Hebditch M, Carballo-Amador MA, Charonis S, Curtis R, Warwicker J. Protein-Sol: A web tool for predicting protein solubility from sequence. Bioinformatics. 2017;33(19):3098–100. doi: 10.1093/bioinformatics/btx345.
24. McGuffin LJ, Bryson K, Jones DT. The PSIPRED protein structure prediction server. Bioinformatics 2000. 16(4):404-5. doi: 10.1093/bioinformatics/16.4.404.
25. Combet C, Blanchet C, Geourjon C, Deléage G. NPS@: Network Protein Sequence Analysis. Bioinformatics. 2000;25(3):147-50. doi: 10.1016/s0968-0004(99)01540-6.
26. Yang J, Zhang Y. I-TASSER server: New development for protein structure and function predictions. Nucleic Acids Res. 2015;43(W1):W174-81. doi: 10.1093/nar/gkv342.
27. Ko J, Park H, Heo L, Seok C. GalaxyWEB server for protein structure prediction and refinement. Nucleic Acids Res. 2012;40(Web Server issue):W294-7. doi: 10.1093/nar/gks493.
28. Wiederstein M, Sippl MJ. ProSA-web: Interactive web service for the recognition of errors in three-dimensional structures of proteins. Nucleic Acids Res. 2007;35(Web Server issue):W407-10. doi: 10.1093/nar/gkm290.
29. Zhu X, Wang X, Liu T, Zhang D, Jin T. Design of multi-epitope vaccine against porcine rotavirus using computational biology and molecular dynamics simulation approaches. Virol J. 2024;21(1):160. doi: 10.1186/s12985-024-02440-9.
30. Jendele L, Krivak R, Skoda P, Novotny M, Hoksza D. PrankWeb: A web server for ligand binding site prediction and visualization. Nucleic Acids Res. 2019;47(W1):W345-9. doi: 10.1093/nar/gkz424.
31. Pettersen EF, Goddard TD, Huang CC, Couch GS, Greenblatt DM, Meng EC, et al. UCSF Chimera - A visualization system for exploratory research and analysis. J Comput Chem. 2004;25(13):1605-12. doi: 10.1002/jcc.20084.
32. Webb B, Sali A. Comparative protein structure modeling using MODELLER. Curr Protoc Bioinformatics. 2016;54:5.6.1–5.6.37. doi: 10.1002/cpbi.3.

33. Abraham MJ, Murtola T, Schulz R, Páll S, Smith JC, Hess B, et al. GROMACS: High performance molecular simulations through multi-level parallelism from laptops to supercomputers. SoftwareX. 2015; 1–2(September 2015):19–25. doi: 10.1016/j.softx.2015.06.001.
34. Yekeen AA, Durojaye OA, Idris MO, Muritala HF, Arise RO. CHAPERON g: A tool for automated GROMACS-based molecular dynamics simulations and trajectory analyses. Comput Struct Biotechnol J. 2023; 21:4849–58. doi: 10.1016/j.csbj.2023.09.024.
35. Vijayamahantesh, Amit A, Dikhit MR, Singh AK, Venkateshwaran T, Das VNR, et al. Immuno-informatics based approaches to identify CD8+ T cell epitopes within the Leishmania donovani 3-ectonucleotidase in cured visceral leishmaniasis subjects. Microbes Infect. 2017;19(6):358–69. doi: 10.1016/j.micinf.2017.03.002.
36. Morel PA, Turner MS. Designing the optimal vaccine: The importance of cytokines and dendritic cell. Open Vaccine J. 2010;3:7–17. doi: 10.2174/1875035401003010007.
37. Abbate MF, Dupic T, Vigne E, Shahsavarian MA, Walczak AM, Mora T. Computational detection of antigen-specific B cell receptors following immunization. Proc Natl Acad Sci U S A. 2024;121(35):e2401058121. doi: 10.1073/pnas.2401058121.
38. Funderburg N, Lederman MM, Feng Z, Grage MG, Jadlowsky J, Harding CV, et al. Human β-defensin-3 activates professional antigen-presenting cells via Toll-like receptors 1 and 2. Proc Natl Acad Sci U S A. 2007;104(47):18631-5. doi: 10.1073/pnas.0702130104.
39. Yang D, Biragyn A, Hoover DM, Lubkowski J, Oppenheim JJ. Multiple roles of antimicrobial defensins, cathelicidins, and eosinophil-derived neurotoxin in host defense. Annu Rev Immunol. 2004;22:181–215. doi: 10.1146/annurev.immunol.22.012703.104603.
40. Dar HA, Waheed Y, Najmi MH, Ismail S, Hetta HF, Ali A, et al. Multiepitope subunit vaccine design against COVID-19 based on the spike protein of SARS-CoV-2: An in silico analysis. J Immunol Res. 2020;2020:8893483. doi: 10.1155/2020/8893483.
41. Hammed-Akanmu M, Mim M, Osman AY, Sheikh AM, Behmard E, Rabaan AA, et al. Designing a multi-epitope vaccine against Toxoplasma gondii: An immunoinformatics approach. Vaccines. 2022;10(9):1389. doi: 10.3390/vaccines10091389.
42. Roy A, Kucukural A, Zhang Y. I-TASSER: A unified platform for automated protein structure and function prediction. Nat Protoc. 2010;5(4):725-38. doi: 10.1038/nprot.2010.5.
43. Suganthi M, Sowmya H, Manjunathan J, Ramasamy P, Thiruvengadam M, Varadharajan V, et al. Homology modeling and protein-protein interaction studies of GAPDH from Helopeltis theivora and chitinase from Pseudomonas fluorescens to control infection in tea (Camellia sinensis (L.) O. Kuntze) plants. Plant Stress. 2024;11(March 2024):100377. doi: 10.1016/j.stress.2024.100377.
44. Krivák R, Hoksza D. P2Rank: Machine learning-based tool for rapid and accurate prediction of ligand binding sites from protein structure. J Cheminform. 2018;10(1):39. doi: 10.1186/s13321-018-0285-8.
45. Krebs BB, De Mesquita JF. Amyotrophic lateral sclerosis type 20: In silico analysis and molecular dynamics simulation of hnRNPA1. PLoS One. 2016;11(7):e0158939. doi: 10.1371/journal.pone.0158939.
46. Sun K, Jia K, Lv H, Wang SQ, Wu Y, Lei H, et al. EBV-positive gastric cancer: Current knowledge and future perspectives. Front Oncol. 2020;10:583463. doi: 10.3389/fonc.2020.583463.
47. Sun Y, Shi D, Sun J, Zhang Y, Liu W, Luo B. Regulation mechanism of EBV-encoded EBER1 and LMP2A on YAP1 and the impact of YAP1 on the EBV infection status in EBV-associated gastric carcinoma. Virus Res. 2024;343:199352. doi: 10.1016/j.virusres.2024.199352.
48. Zhang Y, Lyu H, Guo R, Cao X, Feng J, Jin X, et al. Epstein–Barr virus-associated cellular immunotherapy. Cytotherapy. 2023;25(9):903-912. doi: 10.1016/j.jcyt.2023.04.003.
49. Wistinghausen B, Dave H, Bollard CM. Adoptive cellular immunotherapy for Epstein–Barr virus-associated lymphoproliferative disease. Ann Lymphoma. 2022; 6(June 2022):1-14. doi: 10.21037/aol-21-43.
50. He H, Lei F, Huang L, Wang K, Yang Y, Chen L, et al. Immunotherapy of Epstein–Barr virus (EBV) infection and EBV-associated hematological diseases with gp350/CD89-targeted bispecific antibody. Biomed Pharmacother. 2023; 163(July 2023):114797. doi: 10.1016/j.biopha.2023.114797.
51. Ojha R, Nandani R, Prajapati VK. Contriving multiepitope subunit vaccine by exploiting structural and

nonstructural viral proteins to prevent Epstein–Barr virus-associated malignancy. J Cell Physiol. 2019;234(5):6437-48 doi: 10.1002/jcp.27380.
52. Dasari V, McNeil LK, Beckett K, Solomon M, Ambalathingal G, Thuy TL, et al. Lymph node targeted multi-epitope subunit vaccine promotes effective immunity to EBV in HLA-expressing mice. Nat Commun. 2023;14(1):4371. doi: 10.1038/s41467-023-39770-1.
53. Yurina V, Adianingsih OR. Predicting epitopes for vaccine development using bioinformatics tools. Ther Adv Vaccines Immunother. 2022;10:1-12. doi: 10.1177/25151355221100218.
54. Jiang HW, Li Y, Zhang HN, Wang W, Yang X, Qi H, et al. SARS-CoV-2 proteome microarray for global profiling of COVID-19-specific IgG and IgM responses. Nat Commun. 2020;11(1):3581. doi: 10.1038/s41467-020-17488-8.
55. Yousaf M, Ullah A, Sarosh N, Abbasi SW, Ismail S, Bibi S, et al. Design of multi-epitope vaccine for Staphylococcus saprophyticus: Pan-genome and reverse vaccinology approach. Vaccines. 2022; 10(8):1192. doi: 10.3390/vaccines10081192.
56. Rahimnahal S, Yousefizadeh S, Mohammadi Y. Novel multi-epitope vaccine against bovine brucellosis: Approach from immunoinformatics to expression. J Biomol Struct Dyn. 2023;41(24):15460–84. doi: 10.1080/07391102.2023.2188962.
57. Lester SN, Li K. Toll-like receptors in antiviral innate immunity. J Mol Biol. 2014;426(6):1246-64. doi: 10.1016/j.jmb.2013.11.024.
58. Rex V, Zargari R, Stempel M, Halle S, Brinkmann MM. The innate and T-cell mediated immune response during acute and chronic gammaherpesvirus infection. Front Cell Infect Microbiol. 2023;13:1146381. doi: 10.3389/fcimb.2023.1146381.
59. Zauner L, Nadal D. Understanding TLR9 action in Epstein–Barr virus infection. Front Biosci. 2012;17(4):1219-31. doi: 10.2741/3982.
60. Zauner L, Melroe GT, Sigrist JA, Rechsteiner MP, Dorner M, Arnold M, et al. TLR9 triggering in Burkitt's lymphoma cell lines suppresses the EBV BZLF1 transcription via histone modification. Oncogene. 2010;29(32):4588-98. doi: 10.1038/onc.2010.203.
61. Zhang X, Chen Y, Wang S, Zhong L, Xiang Z, Zhang X, et al. TianTan vaccinia virus-based EBV vaccines targeting both latent and lytic antigens elicits potent immunity against lethal EBV challenge in humanized mice. Emerg Microbes Infect. 2024;13(1):2412640. doi: 10.1080/22221751.2024.2412640.
62. Fatahi G, Abdollahi M, Nashtahosseini Z, Minoo S, Mostafavi M, Saeidi K. Designing of an efficient DC-inducing multi-epitope vaccine against Epstein–Barr virus targeting the GP350 using immunoinformatics and molecular dynamic simulation. Biochem Biophys Rep. 2025;42:101966. doi: 10.1016/j.bbrep.2025.101966.
63. Deepthi V, Sasikumar A, Mohanakumar KP, Rajamma U. Computationally designed multi-epitope vaccine construct targeting the SARS-CoV-2 spike protein elicits robust immune responses in silico. Sci Rep. 2025;15(1):9562. doi: 10.1038/s41598-025-92956-z.
64. Allemailem KS. In silico development of a chimeric multi-epitope vaccine targeting Helcococcus kunzii: Coupling subtractive proteomics and reverse vaccinology for vaccine target discovery. Pharmaceuticals. 2025;18(9):1258. doi: 10.3390/ph18091258.